Field-scale CH_4 emission at a sub-arctic mire with heterogeneous permafrost thaw status

Patryk Łakomiec[1], Jutta Holst[1], Thomas Friborg[2], Patrick Crill[3], Niklas Rakos[4], Natascha Kljun[5], Per-Ola Olsson[1], Lars Eklundh[1], Andreas Persson[1], Janne Rinne[1]

[1] Department of Physical Geography and Ecosystem Science, Lund University, 223 62, Sweden

[2] Department of Geosciences and Natural Resource Management, University of Copenhagen, 1165, Denmark

[3] Department of Geological Sciences and Bolin Centre for Climate Research, Stockholm University, 114 19, Sweden

[4] Abisko Scientific Research Station, Swedish Polar Research Secretariat, Abisko, 981 07, Sweden

[5] Centre for Environmental and Climate Science, Lund University, 223 62, Sweden

Correspondence to: Patryk Łakomiec (patryk.lakomiec@nateko.lu.se)

Abstract

The Artic is exposed to even faster temperature changes than most other areas on Earth. Constantly increasing temperature will lead to thawing permafrost and changes in the methane (CH_4) emissions from wetlands. One of the places exposed to those changes is the Abisko-Stordalen Mire in northern Sweden, where climate and vegetation studies have been conducted since the 1970s.

In our study, we analyzed field-scale methane emissions measured by the eddy covariance method at Abisko-Stordalen Mire for three years (2014-2016). The site is a subarctic mire mosaic of palsas, thawing palsas, fully thawed fens, and open water bodies. A bimodal wind pattern prevalent at the site provides an ideal opportunity to measure mire patches with different permafrost status with one flux measurement system. The flux footprint for westerly winds is dominated by elevated palsa plateaus, while the footprint is almost equally distributed between palsas and thawing bog-like areas for easterly winds. As these patches are exposed to the same climatic and weather conditions, we analyzed the differences in the responses of their methane emission for environmental parameters.

The methane fluxes followed a similar annual cycle over the three study years, with a gentle rise during spring and a decrease during autumn, without emission burst at either end of the ice-free season. The peak emission during the ice-free season differed significantly for the mire with two permafrost status: the palsa mire emitted 19 mg-C m^{-2} d^{-1} and the thawing wet sector 40 mg-C m^{-2} d^{-1}. Factors controlling the methane emission were analyzed using generalized linear models. The main driver for methane fluxes was peat temperature for both wind sectors. Soil water content above the water table emerged as an explanatory variable for the three years for western sectors and the year 2016 in the eastern sector. The water table level showed a significant

correlation with methane emission for the year 2016 as well. Gross primary production, however, did not show a significant correlation with methane emissions.
Annual methane emissions were estimated based on four different gap-filing methods. The different methods generally resulted in very similar annual emissions. The mean annual emission based on all models was 3.1 ± 0.3 g-C m^{-2} a^{-1} for the western sector and 5.5 ± 0.5 g-C m^{-2} a^{-1} for the eastern sector. The average annual emissions, derived from these data and a footprint climatology, were 2.7 ± 0.5 g-C m^{-2} a^{-1} and 8.2 ± 1.5 g-C m^{-2} a^{-1} for the palsa and thawing surfaces, respectively. Winter fluxes were relatively high, contributing 27 - 45 % to the annual emissions.

1 Introduction

After a period of stabilization in the late 1990s to early 2000s, atmospheric methane (CH_4) concentration is increasing again at rates similar to those before 1993, which is approximately 12 ppb yr^{-1} (Dlugokencky et al. 2011, Nisbet et al. 2014, Saunois 2020). The reasons behind this increase are still partly unclear, as the mechanisms that control the global CH_4 budget are not completely understood (Kirschke et al. 2013, Saunois et al. 2020). The largest natural source of CH_4 are wetlands, based on top-down emission estimates (Saunois et al. 2020), and this source may become stronger in the warming climate (Zhang et al. 2017). The shift in the isotopic composition of CH_4 towards more negative values also supports the hypothesis of changes in the biological source strength driving the increase in CH_4 concentration, as atmospheric CH_4 is becoming more ^{13}C-depleted (Nisbet et al. 2016).

Increasing temperature has shown to speed up the degradation of permafrost which leads to losses in the soil carbon pool, often in the form of carbon dioxide (CO_2) and CH_4 (Malmer et al. 2005). The high northern latitudes are experiencing the fastest temperature increase due to the ongoing global warming. Temperature changes in the Arctic have been twice as high as the global average (Post et al. 2019).

Ecosystems near the annual near-surface air temperature isotherms of 0 °C are vulnerable to permafrost thaw and changes in ecosystem characteristics in a warming climate. These vulnerable ecosystems include palsa mires, such as Stordalen Mire near Abisko, Sweden, where the recent warming has led to annual average temperatures exceeding 0 °C since 1980s (Callaghan et al. 2010, Callaghan et al. 2013, Post et al. 2019, Figure S1). The warming has led to an acceleration of permafrost thaw processes and a transition from palsa plateaus, underlain by permafrost, to non-permafrost fen systems (Malmer et al. 2005). These deviations are likely to induce changes in biogeochemical processes, including increased CH_4 emissions (Christensen et al. 2003).

The most direct micrometeorological field-scale method used to measure CH_4 exchange between ecosystem and atmosphere is the eddy covariance (EC) method (e.g. Verma et al. 1986, Aubinet et al., 2012). The advantages of this method are its high temporal resolution and minimal disturbance to the measured surface. Thus, it is feasible for long-term measurements of rates of gas exchange that integrates over surface variation (Knox et al. 2016, Li et al. 2016, Rinne et al.

2018). However, information on the small-scale spatial distribution of surface fluxes is lost with the method due to the spatially integrative nature of the EC method. Instead of resolving the small-scale spatial variability, the EC method provides averaged fluxes from a larger area, the flux footprint area (Kljun et al. 2002). However, spatial variability can be resolved by the EC method using measurements conducted under different wind directions, as the footprint area is located upwind of the measurement tower. We can take advantage of this feature to obtain gas exchange rates from two different ecosystem types with one measurement system by placing the measurement system on the border between these systems (e.g. Jackowicz-Korczyński et al., 2010; Kowalska et al., 2013; Jammet et al., 2015; 2017). Stordalen Mire offers an excellent opportunity to conduct flux studies where one flux system is used to monitor two ecosystem types since the wind direction is bimodal. While previous studies in the area have compared open water surfaces to completely thawed fen (Jammet et al., 2015, 2017, Jansen et al. 2020), no comparison of field-scale CH_4 emission between permafrost palsa plateaus and thawing wet areas has been conducted yet.

Previous studies on CH_4 emission within the Stordalen Mire from areas with different permafrost status have been done using chamber measurements (McCalley et al. 2014, Deng et al. 2014). McCalley et al. (2014) reported CH_4 emissions from palsas underlain by permafrost to be close to zero, summertime emissions from thawing wet areas to be around 25 mg-C m^{-2} d^{-2}, while completely thawed fen sites revealed much higher emission of 150 mg-C m^{-2} d^{-2}. There are only few wintertime data on CH_4 emission available using the chamber method (Christensen et al. 2000, Nilsson et al. 2008, Godin et al. 2012, McCalley et al. 2014). However, EC measurements conducted at different northern mires typically show low but positive emissions in winter (Rinne et al., 2007; Yamulki et al. 2013, and others).

In this study we analyzed field-scale CH_4 emission from two areas of Stordalen subarctic mire. The first area is dominated by drained permafrost plateau. The second area is thawing and thus resulting in wetter conditions. Outputs from this analysis are differences in the CH_4 emissions from the mire patches with heterogeneous permafrost status. We are expecting, based on the previous studies, that fluxes from the wetter sector will be around 30 mg-C m^{-2} d^{-2}, while the palsa plateau will emit significantly lower fluxes during the peak season. We presume that winter fluxes will be positive but very low.

For estimation of annual CH_4 emission we need gap-free datasets. Up to date, there is no generally accepted gap-filling method for CH_4 fluxes, hence four different gap-filling methods were compared. The test of the four methods will decrease the uncertainty in the annual balance estimation (Hommeltenberg et al. (2014), Rößger et al. (2019), Kim et al. (2019)). It was important to use more than one method in this case of study because datasets were portioned and due to that contained more gaps.

This study aimed to estimate the annual CH_4 emission from two distinct different ecotypes, with heterogeneous permafrost status, exposed to the same environmental factors. Furthermore, we

115 analyzed the seasonal cycle of CH_4 emission to quantify the contribution during different seasons.
116 Moreover, an analysis of differences in controlling factors for these two different areas was done.
117

118 2 Materials and method

119 2.1 Study site

120 The study area is Stordalen Mire, a mire complex underlain by discontinuous permafrost located
121 in northern subarctic Sweden (68°20' N, 19°30' E) near Abisko (Ábeskovvu). The station Abisko-
122 Stordalen (SE-Sto) is a part of the ICOS Sweden research infrastructure and is the only one in
123 Sweden situated in the subarctic region. The measurement period that is analyzed here covers
124 three years from 2014 to 2016. The mean annual near- surface air temperature in this region has
125 been increasing during the last decades, and temperatures recorded by SMHI (Sveriges
126 meteorologiska och hydrologiska institut) at ANS (Abisko Naturvetenskapliga Station) has
127 exceeded the 0 °C threshold since the late 1980s (Callaghan et al. 2013, Figure S1). During the
128 years 2014-2016, the mean near-surface air temperature (Ta) was 1.0 °C and 0.3 °C at ANS and
129 the ICOS Sweden station Abisko-Stordalen (SE-Sto), respectively. The average annual
130 precipitation, based on ANS data, is around 330 mm yr^{-1}. An acceleration of permafrost loss with
131 increasing temperatures is likely (Callaghan et al. 2013).
132 The large mountain valley of Lake Torneträsk (Duortnosjávri) channels winds at the study site,
133 leading to a bimodal wind distribution (Figure 1), which allows us to divide our analyses into two
134 distinct sectors. The plant community structure around the tower is determined by the hydrology
135 which in turn is determined by the microtopographic variation in the surface due to the local
136 permafrost dynamics. Different plant communities would have different productivities thus
137 controlling the CO_2 and CH_4 fluxes from those surfaces. The area to the west of the EC mast is
138 dominated by a drier permafrost palsa plateau hereafter referred to as the western sector,
139 whereas the area to the east is a mixture of thawing wet areas and palsas, hereafter referred to
140 as the eastern sector. The drained permafrost plateau is dominated by *Empetrum*
141 *hermaphroditum*, *Betula nana*, *Rubus chamaemorus*, *Eriophorum vaginatum*, *Dicranum*
142 *elongatum*, *Sphagnum fuscum*. The wet areas are characterizing by *E. vaginatum*, *Carex*
143 *rotundata*, *S. balticum*, *Drepanucladus schulzei*, *Politrichum jensenii* (Johansson et al. 2006). The
144 thawing areas in this sector exhibit ombrotrophic, bog-like, features. Dominant vegetation varies
145 with the microforms of the mire.
146

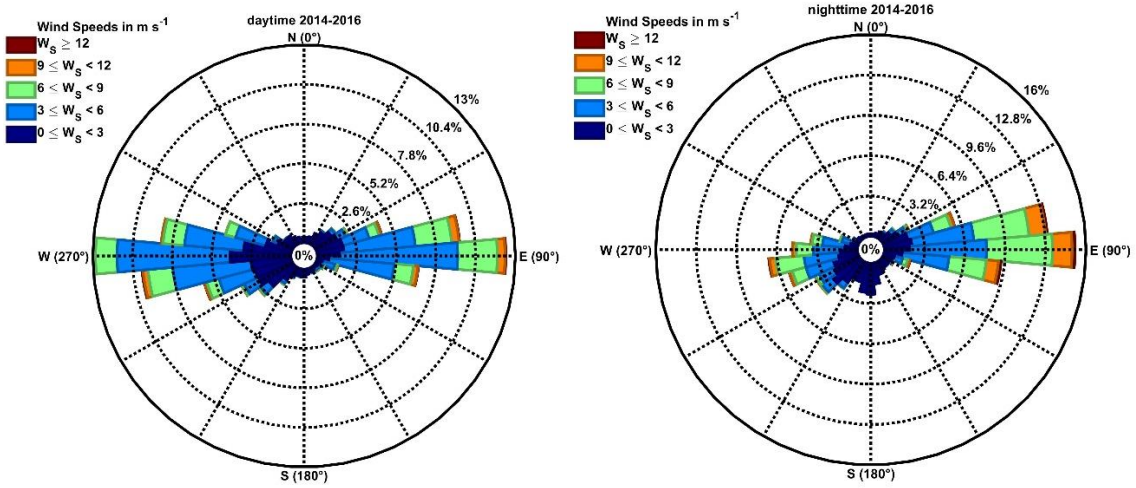

147

148 Figure 1. The wind rose for SE-Sto tower for years 2014-2016 for the daytime (left panel) and nighttime
149 (right panel)

150

151

152 ## 2.2 Flux measurements

153 The EC measurements of CH_4 fluxes at SE-Sto are made using a closed-path fast off-axis
154 integrated cavity output spectrometer (OA-ICOS LGR model GGA-24EP, ABB Ltd, Zurich,
155 Switzerland) combined with a 3-D sonic anemometer (SA-Metek uSonic-3 CLASS A, Metek GmbH,
156 Germany). Air was sampled via a 29.6 m long polyethylene tubing with an 8.13 mm inner
157 diameter. Analysis of the high-frequency loss were performed to assess the effect of relatively
158 long sample tubing. We analyzed this with the co-spectra of the CH_4 and the vertical wind speed
159 w. The analysis did not show a dampening effect at the high frequencies (Figure S2), thus the high
160 frequency attenuation does not seem to be very large. Furthermore, the post-processing
161 software we used to calculate fluxes includes correction for high-frequency losses. The nominal
162 tube flow rate was 36 l min^{-1}. The sampling inlet was displaced 22 cm horizontally of the sonic
163 anemometer measurement volume towards 180°. The response time of the LGR-FGGA was 0.1 s.
164 The LGR FGGA was placed inside a heated and air-conditioned shelter. The anemometer was
165 located north of the instrument shelter and was oriented with the sensors north pointing towards
166 186°. This orientation allows undisturbed wind measurements from both main wind directions,
167 East and West.
168 CO_2 and H_2O were measured with a LI-COR LI-7200 (LI-COR Environment, USA) closed path infra-
169 red gas analyzer. The sampling inlet was at the same location as the sampling point for the CH_4
170 analyzer. Sampled air was transported through 1.05 m and of 5.3 mm ID tubing. The nominal
171 tube flow rate was 15 l min^{-1}.

172 The anemometer and air sampling tubes were mounted on a mast of 2.2 m above ground level
173 (a.g.l.) (68°21'21.32" N, 19°2'42.75" E), placed at the edge of the western and the eastern sectors.

Data were collected by an ISDL data logger (In Situ Instrument AB, Sweden) with a 20 Hz time resolution.

2.3 Ancillary Measurements

Ancillary measurements are presented in Table S1. The sampling frequency for these parameters was 1 Hz and the collected data were averaged into half-hourly values. Measured variables are divided into two categories: peat/soil parameters, and meteorological parameters. Peat temperatures at each depth, soil heat fluxes, and soil water contents (SWC) were measured at four locations around the EC tower, located towards the four cardinal directions. In further analysis, data just from two of these locations were used (East and West) as these were within the flux footprint areas of the EC tower. The sites for the water table level (WTL) measurements differed from the peat temperature profiles. The soil pit for temperature and moisture probe in the western sector is located on a palsa plateau. However, the WTL probe is located in a pond approximately 10 m away from the soil temperature and SWC measurement, as there is no WTL above the permafrost of palsas. The soil pit for temperature and SWC probe in the eastern sector is located in the wet thawing area. The WTL probe is located in the wetter area approximately 10 m away. Furthermore, data for WTL was available only during the unfrozen period, as the probes were removed during the frozen period to avoid damage. Meteorological variables were measured on a separate mast, placed 10 meters south-west of the flux measurement mast.

2.4 Flux calculation

Fluxes of CO_2, CH_4, H_2O, and sensible heat were calculated using EddyPro 6.2.1 (LI-COR Environment, USA) as half-hourly averages. The data quality flagging system and advanced options for EddyPro were set up following Jammet et al. (2017). The wind vector was rotated by a double rotation method and data were averaged by block averaging (Aubinet et al. 2012). The time lag was obtained by maximizing the covariance (Aubinet et al. 2012).

Based on the wind direction, the half-hourly data were divided into western and eastern datasets, similarly to analyses by Jackowicz-Korczyński et al. (2010) and Jammet et al. (2015, 2017). The eastern dataset contained fluxes and other variables recorded when the wind was from 45°-135°, and the western dataset parameters when wind directions were 225°-315°. These two datasets were analyzed separately. Fluxes measured with wind from these two sectors are influenced by mire surfaces dominated by differing permafrost status, moisture regimes, and plant community structures. These reflect the thaw stages of a dynamic arctic land surface, responding to the warming climate. These two wind sectors include more than 80 % of all data during the years 2014-2016. Northerly and Southerly wind directions, i.e. winds from outside these sectors occurred mainly in low wind speed conditions. The distribution of wind directions is presented in Figure 1.

CH_4 fluxes were filtered by quality flags according to Mauder and Foken (2004). These indicate the quality of measured fluxes, "0" being the best quality fluxes, "1" being usable for annual budgets, and "2" being flux values that should not be used for any analysis. Thus, in further analysis fluxes with flag "2" were removed. Also, consecutive data points originating from the two pre-defined wind direction sectors were removed to avoid influences from non-stationary conditions. We also analyzed the behavior of the CH_4 fluxes against low turbulence conditions using friction velocity (u*) as a measure of turbulence. We binned the CH_4 fluxes into 0.05 m s^{-1} u* bins and plotted the binned CH_4 flux values against u* in 40-day windows over the growing period (d.o.y. 150-250, d.o.y. 210 was the beginning of the last averaging window). The CH_4 flux showed no dependence on u* below 0.6 m s^{-1}. A slight positive correlation was found during stronger turbulent conditions (u* > 0.6 m s^{-1}), but we deemed this not high enough to warrant exclusion of those points from further analysis. Thus, we did not remove data based on the results of u*. The fraction of data remaining, after filtering based on the quality flags and other criteria described above, is presented in Table 2.

The analysis of relations of CH_4 fluxes to environmental parameters was done using the non-gap-filled dataset of daily averages, to avoid the danger of circular reasoning of analyzing the relations to the same factors that were used for gap-filling.

2.5 Footprint modeling and land cover classification

A detailed land cover classification was performed for the EC-tower footprint area to estimate the flux contribution from the drained palsa and the thawing wet areas. We used images over the Stordalen Mire collected with an eBee (SenseFly, Lausanne, Switzerland) Unmanned Aerial Vehicle (UAV) carrying a Parrot Sequoia camera (Parrot Drone SAS, Paris, France) on July 31, 2018. The images were processed in Agisoft Photoscan (Agisoft LLC, St. Petersburg, Russia) to create an orthomosaic and a Digital Surface Model (DSM) with spatial resolutions of 50 cm x 50 cm. Field data for training a classification were collected in mid-August 2018 with sampling areas of 50 cm × 50 cm that were classified into wet or dry, and a random forest classification was performed to classify the footprint into wet and dry areas with the orthomosaic and DSM as input. The dry areas in the flux footprint areas of SE-Sto footprint correspond to palsas, while the wet areas are thawing surfaces.

Flux footprints were calculated with the FFP model (Kljun et al. 2015). Receptor height, Obukhov length, standard deviation of lateral velocity fluctuations, friction velocity, and roughness length were used as input data. The input data were divided into the two wind sectors mentioned above, before footprint calculation, and footprints were calculated separately for them. We calculated footprints for each half-hourly data point and aggregated these to annual footprint climatologies for each sector separately. I.e. the half-hourly footprint function values were aggregated for each land cover grid cell (50 cm x 50 cm) to derive a footprint-weighted flux contribution per pixel.

Based on the land cover classification and annual CH_4 fluxes for each sector, combined and weighted with the footprint climatology, it was possible to estimate annual emissions from the different surface type.

2.6 Gap-filling methods for CH_4

We compared four different gap-filling methods, separately for both sectors. These methods were: look-up tables (REddyProc ("Jena gap-filling tool"), Wutzler et al. 2018), 5-day moving mean, artificial neural network (Jammet et al. 2015, 2017), and generalized linear models (Rinne et al. 2018). All these methods, except for moving mean, have been used before for gap-filling CH_4 flux data from different mire ecosystems. The look-up table approach uses half-hourly data, while for the other three methods we used daily average data, as CH_4 emissions from this ecosystem do not show a diel cycle (see below, Section 3.2 for a detailed description).

The uncertainties due to each method were analyzed by the introduction of artificial gaps to the data, with lengths comparable to gaps existing in the year 2014. 35-day and 80-day gaps were implemented to the data of years 2015 and 2016. Gaps were placed in the winter period, to obtain similar gap distribution as in the year 2014 (gap distribution is presented below in Table 3). Annual sums, with artificial gaps, were compared with results from methods without those gaps. Statistical significances of differences between models were analyzed by using a two-sample t-Test for equal means with a 95 % confidence level (MATLAB R2019b).

2.6.1 REddyProc

The Jena gap-filling tool using look-up tables requires half-hourly data of CH_4 flux and environmental data: shortwave incoming radiation, air temperature, soil temperature, relative humidity, and friction velocity. Based on environmental data, fluxes are classified and averaged within a given time window. The missing data are then filled with the average value from classified data. Uncertainty can be estimated as standard deviations of fluxes within classes. Detailed information about the method is presented by Falge et al. (2001) and Wutzler et al. (2018).

2.6.2 Moving average

A 5-day moving mean approach is a very simple gap-filling method where the moving mean is calculated for subsets of the data. In case of a gap in the averaging window, the mean value is calculated for fewer observations. The method was applied on daily average CH_4 flux data using MATLAB (movmean function). For gaps longer than 5 days, linear interpolation was used between the last point before the gap and the first point after gap. Uncertainties of the single gap-filled flux were estimated by calculating the moving standard deviation (movstd function, MATLAB) on the same subset of the data like for the moving mean.

2.6.3 Artificial Neural Network

An artificial neural network (ANN) has been successfully applied for gap-filling of CH_4 fluxes by e.g. Dengel et al. (2013), Jammet et al. (2015,2017), Knox et al. (2016) *and* Rößger et al. (2019). This type of ANN was designed in MATLAB using a fitnet function with 30 hidden neurons. We used the Levenberg-Marquardt algorithm as a training function (Levenberg 1944 Marquardt 1963). All available daily average CH_4 values were used to train (70 %), validate (15 %), or test (15 %) the ANN. The ANN requires input data without gaps to work properly and thus the short gaps (up to three days) in environmental daily averaged data were filled by linear interpolation before the ANN analysis. All environmental variables, except the WTL were used as input for the ANN method. The WTL was excluded because it was not available during the frozen period, i.e. most of the year. The ANN method was applied to sectors and each year separately (ANN YbY) or all three years together. Multiple repetitions were done to minimize uncertainty connected with randomly chosen data points for training, validation, and testing. The network was trained and used to calculate the time series of CH_4 daily fluxes 100 times in each case of gap-filling. The number of repetitions was chosen to have a sample large enough to calculate reliable mean and standard deviation values, and to keep the computation time reasonably short. An average CH_4 flux for each day was calculated based on 100 daily values. The gaps in the measured flux time series were filled with values from the time series calculated by ANN. Errors were estimated as standard errors of mean on daily flux, based on 100 ANN trained values.

2.6.4 Generalized Linear Model

Generalized linear models (GLM) are linear combinations of linear and quadratic functions describing the dependence of response variables to predictors. In our case, the response variable was the logarithm of daily average CH_4 flux, and predictors were daily averages of measured environmental variables. Controlling factors of CH_4 emission were examined by a procedure similar to the routine described by Rinne et al. (2018). A correlation matrix of linear correlation based on daily values of environmental factors and CH_4 fluxes was constructed (Figure S3). Additionally, the logarithm of CH_4 fluxes was added to the correlation matrix to check the exponential relationship between parameters. This type of relationship between CH_4 fluxes and peat temperature was previously found by e.g. Christensen et al. (2003), Jackowicz-Korczyński et al. (2010), Bansal et al. (2016), Pugh et al. (2017) and Rinne et al. (2018). Gap-filled CO_2 flux, and gross primary production (GPP), were also included as prospective controlling factors. In order to avoid strong cross-correlation between predictors, first, we selected the parameter with the highest correlation and then removed parameters from the GLM development with a cross-correlation between parameters $R^2 > 0.6$. We thus chose GPP, soil temperature at 30 cm depth for the eastern sector and 10 cm depth for the western sector, soil water content (SWC), short-wave incoming radiation, and vapor pressure deficit (VPD) as possible predictors. The model was constructed in MATLAB using the stepwiseglm function (Dobson 2002). The GLM was made

separately for each year (GLM YbY) and for all three years combined. Errors were estimated as 95 % confidence intervals because it was an output of the stepwise function. This method was also used for the determination of the controlling factors from the possible predictors.

2.7 Gap-filling of CO_2 fluxes

CO_2 fluxes were calculated for both wind sectors. CO_2 flux exhibited a diel pattern in the growing season, with uptake during daytime (shortwave incoming radiation > 50 W m^{-2}) and release at night (shortwave incoming radiation < 50 W m^{-2}). We used the ANN to gap-fill the time series of CO_2 fluxes. This method was chosen to check the possibility to reconstruct the diel cycle. This diel pattern of CO_2 was taken into account by using half-hourly data. We used all environmental variables excluding the WTL, as for CH_4 fluxes. GPP was obtained by partitioning the gap-filled data using the Jena gap-filling tool. Finally, the half-hourly gap-filled GPP and CO_2 data were averaged to daily values.

2.8 Contribution of palsa and thaw surfaces to average CH_4 emission

Using the average annual CH_4 emission from the two wind sectors and the relative contributions of the two surface types to the fluxes from these sectors, we calculated the average annual emission from these surface types. We expressed the average annual CH_4 fluxes for the two sectors, F_e (East) and F_w (West), with a pair of equations,

$$F_e = f_{e,p}E_p + f_{e,t}E_t, \quad (1)$$

$$F_w = f_{w,p}E_p + f_{w,t}E_t, \quad (2)$$

where f indicates the fractional contribution of surface type to the flux from the footprint calculations (subscripts *e* and *w* referring to east and west, respectively; *p* and *t* to palsa and thaw surface, respectively); and E_p and E_t are emissions from palsa and thaw surface, respectively. We solved this equation set with two unknowns to yield E_p and E_t. Here we assumed that the emission rate from both palsa and thaw surfaces are equal in eastern and western sectors. Furthermore, we must assume that there is no correlation between footprint contribution and seasonally developing emission rate at either surface type. The seasonally constant contributions of the surface types to the footprint indicate that the latter assumption may well be valid (Figure S4).

2.9 Definition of seasons

The beginning of the unfrozen period was defined as the day when daily averages of peat temperature at 10 cm depth had been above 0 °C for three consecutive days. The end of the unfrozen period was defined as the day when daily averages of peat temperature at 10 cm depth had been below 0 °C for three consecutive days. The unfrozen and frozen periods commence in the western sector on average 3 days earlier than in the eastern sector, but differences in the unfrozen season length are not systematic (Figure 2). The beginning and the end of the unfrozen

season were determined independently for both sectors. The horizontal distance between soil temperature sensors in eastern and western sectors was around 75 m, differed about 2 m in elevation, and the distance from the flux tower was roughly 40 m.

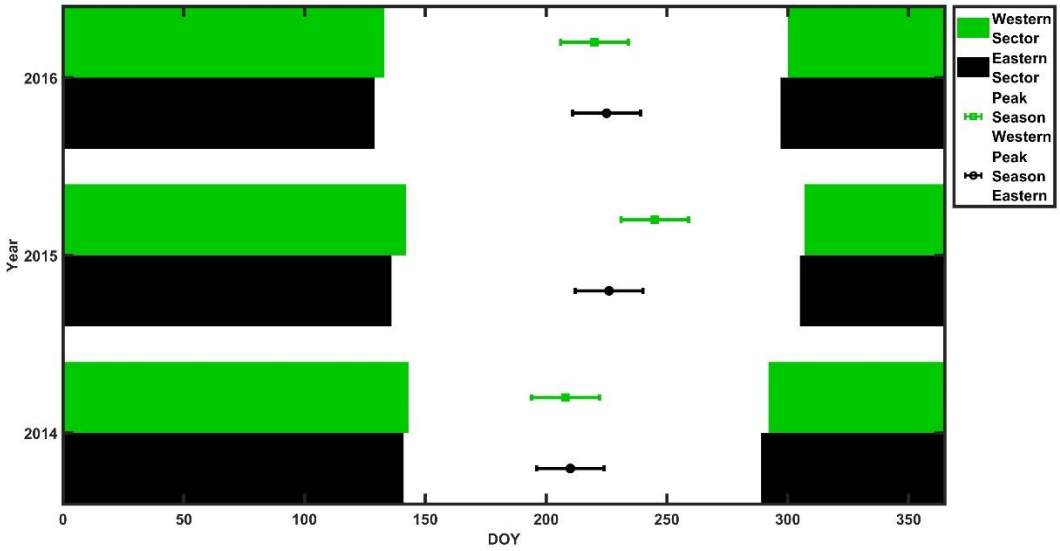

Figure 2. Time periods of frozen peat during the years 2014 - 2016 (green and black bars) and peak CH_4 emission season (dot with whiskers) for the western sector (green) and the eastern sector (black). (For peak season definition see Section 3.2)

3 Results

3.1 Environmental conditions and flux footprints

Winds from eastern and western sectors contributed to 50 % and 40 % to the daytime wind directions, respectively (Figure 1). Northerly and southerly winds contributed to around 5 % each. In the nighttime, 51 % of wind was from the East and 32 % from the West. Additionally, 15 % of total wind came from the South during nighttime, probably as catabatic flow from higher mountain areas. The wind from North was rare, around 2 % of all the cases.

The annual average peat temperature of the uppermost 50 cm of peat was systematically warmer in the eastern sector than in the western sector (Table 1; Figure 3). However, the summertime peat temperature at the top 10 cm layer was warmer for the western sector (Figure S5). The situation was the opposite during winter when the western sector down to 50 cm was colder than the eastern sector. During our investigation period (2014-2016), the peat temperatures from 30 cm to 50 cm below ground were colder in the western sector than those of the eastern sector, corresponding to the existence of the permafrost. Temperature differences, between both areas, at the same depth, were stable over the measurement years. The biggest difference

was noticed at a depth of 30 cm. The temperatures at 30 cm and 50 cm depth were increasing during consecutive years.

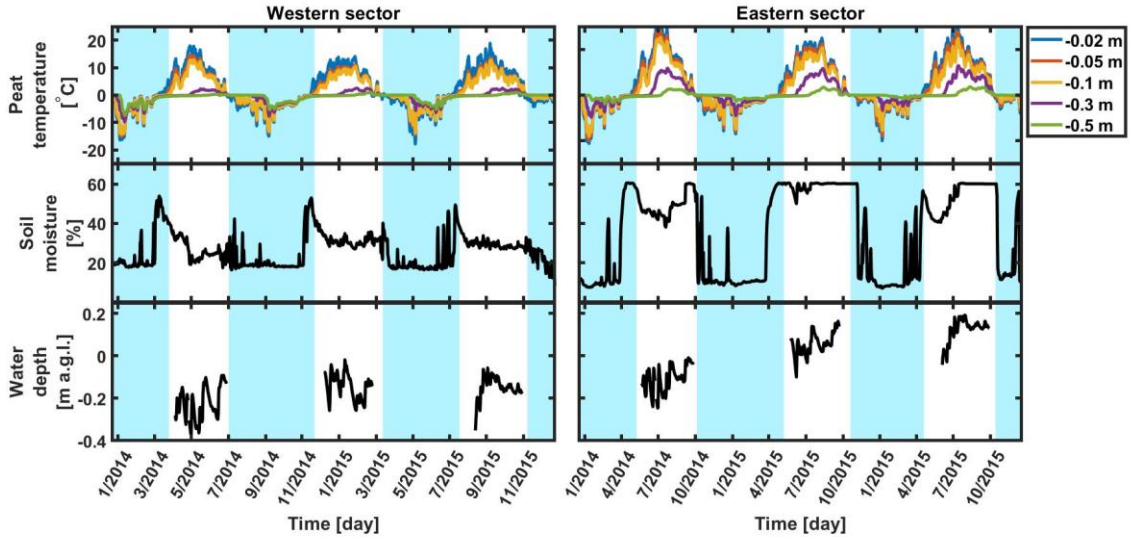

Figure 3. Time series of daily mean values for western and eastern sectors for: peat temperature (top panel), soil moisture (middle panel), and water table level (bottom panel), where the shaded light blue area is the frozen period, when peat temperature at 10 cm was below 0 °C (see Section 2.8 for a detailed description).

Table 1. Mean annual air and peat temperatures for the years 2014-2016 for eastern and western sectors.

	Temperature [°C]								
depth in cm	2014 E	2014 W	2014 E-W difference	2015 E	2015 W	2015 E-W difference	2016 E	2016 W	2016 E-W difference
ambient air	0.3	0.3	-	0.1	0.1	-	0.3	0.3	-
2	1.6	1.4	0.2	2.2	2.0	0.2	2.2	1.9	0.2
5	1.4	0.8	0.5	1.9	1.3	0.7	1.9	1.3	0.6
10	1.2	0.5	0.6	1.7	1.1	0.7	1.7	1.1	0.6
30	0.3	-0.9	1.2	0.6	-0.6	1.2	0.8	-0.5	1.3
50	-0.1	-1.0	0.8	0.0	-0.8	0.8	0.2	-0.6	0.8

The WTL was higher in 2014 than in 2015 and 2016 according to measurements both in the eastern and western sectors (Figure 3). This is not reflected in the SWC measurements, which is

probably due to the different locations of the measurements of WTL and SWC. In the western sector the WTL was measured in an isolated wet patch, surrounded by drier palsa and thus it is not representative of the dominating type of this area. The WTL in the eastern sector was more representative of the area of the footprint. Data from the WTL probe in the West part of the mire was excluded from the further analysis as it does not represent the situation for the majority of the western sector. The soil moisture was higher for the eastern than the western sector during all years. The data shows a distinctive step change at thaw and freeze, as the dielectricity of ice and liquid water differ. In the eastern sector, the soil was fully saturated for most of the unfrozen period during the years 2015-2016, while 2014 indicates lower water content levels. The western sector was never fully saturated at any time during the years 2014-2016.

Footprint and flux contribution of drier and wetter areas are presented in Figure 3. The dry areas (yellow) contribute on average over all three years to more than 90% of the fluxes measured from the western sector at the eddy covariance tower. In the eastern sector, the wetter (blue) and drier areas contribute almost equally to the fluxes. The contributions of the wet and dry areas to the fluxes in both sectors remained almost constant across the three study years.

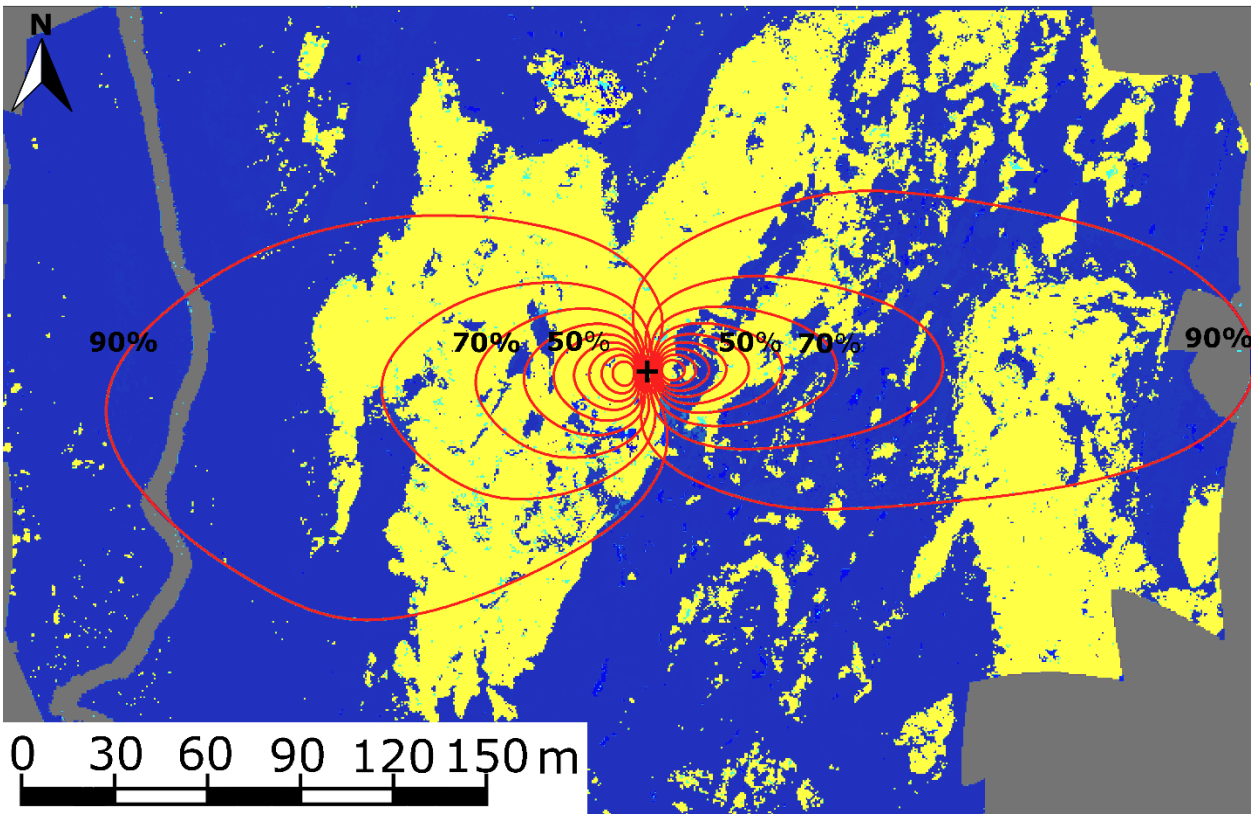

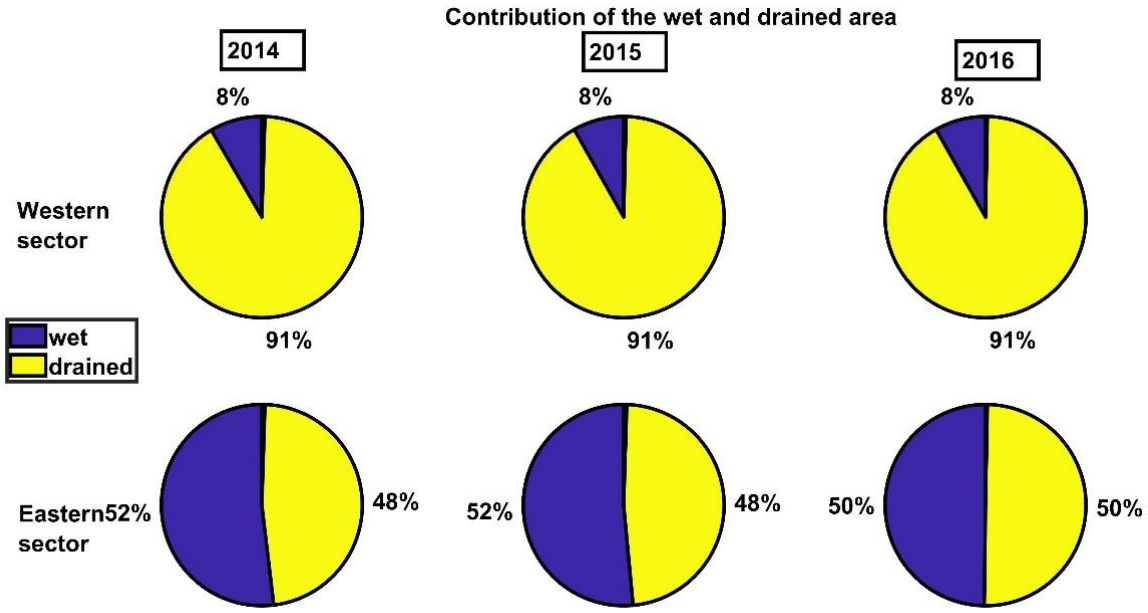

Figure 4. Footprint-weighted contribution of the wet and drained area at the SE-Sto tower (upper panel) for the year 2014 and relative amounts of wetter areas (blue) and drained palsa area (yellow) inside the 80 % area of influence of the footprints (lower panel). The black cross is the location of the tower and each red line indicates 10 % of the contribution from the source area to measured fluxes at the tower. The footprint climatology is almost identical for all study years, see bottom panel.

3.2 CH_4 fluxes

We analyzed the growing season data of each year and both wind sectors separately in regards to a possible diel cycle of CH_4 fluxes. This was done by normalizing each half-hourly flux by dividing it with the daily median from that day for the whole growing season (Rinne et al. 2007). This yielded a normalized diel cycle of CH_4 fluxes. Figure S6 shows slightly lower emission during mid-day hours. However, the difference is small compared to the short term variation in the fluxes as indicated by the interquartile range. Thus, for the purpose of gap-filling this effect could be negligible in calculating daily averages. However, it is interesting to observe this type of diel cycle, with minima at daytime. It could be linked to the temperature cycle of the top peat layer. This could affect the methanotrophy, while the methanogenesis occurring at slightly deeper layers would be less affected. This would lead to higher methanotrophy at daytime and thus lower emission. It is possible to calculate CH_4 daily averages without gap-filling the diel cycle, similarly to e.g. Rinne et al., (2007, 2018) and Jackowicz-Korczyński et al. (2010). We discarded daily averages with less than 10 flux data points from further analysis, to ensure the reliability of the daily average fluxes. Uncertainties of daily averages were calculated as standard errors of the mean. The size of the available flux dataset, after gap-filling by daily averaging, is presented in Table 2. The gap distribution in the datasets for the different sectors and years is presented in Table 3.

441

442 Table 2. The size of available daily data sets after gap-filling by daily averaging for each year and
443 wind sector.

	2014 E	2015 E	2016 E	2014 W	2015 W	2016 W
total number of points	*365*	*365*	*366*	*365*	*365*	*366*
number of points after averaging	*137*	*174*	*182*	*96*	*167*	*178*
% of available data	*38*	*48*	*50*	*26*	*46*	*49*
% of available data during winter period	*36*	*54*	*56*	*12*	*36*	*37*
% of available data during unfrozen period	*40*	*41*	*42*	*47*	*58*	*63*

444

445 Table 3. Gaps distribution over years and wind direction.

Type of gap	Length of gap	2014 E	2015 E	2016 E	2014 W	2015 W	2016 W
short gap	1-3 day	*32*	*50*	*41*	*24*	*44*	*36*
medium gap	4-7 day	*7*	*12*	*11*	*6*	*8*	*11*
long gap	8-30 day	*3*	*7*	*4*	*4*	*6*	*6*
very long gap	> 30 day	*1*	*0*	*0*	*3*	*0*	*0*

446

447 Daily non-gap-filled CH_4 fluxes showed a characteristic annual cycle, with peak emissions in
448 August (Figure 5) and low but positive wintertime fluxes. Wilcoxon rank sum test need data
449 without autocorrelation. The autocorrelation in the data existed up to 8 days. Based on this we
450 divided winter data with subsets where every 9th day was selected. We tested the difference of
451 those subsets to zero with Wilcoxon rank sum test. Winter fluxes were statistically different from
452 zero ($p < 0.001$, two-sided Wilcoxon rank sum test). Winter fluxes from the western and eastern
453 sectors were also different from each other ($p < 0.001$).

454 CH_4 fluxes, both from the western sector and the eastern sector started increasing after
455 snowmelt up to a maximum in August (Figure 5). No major springtime emission burst nor autumn
456 freeze-in burst were observed in any of the years.

457

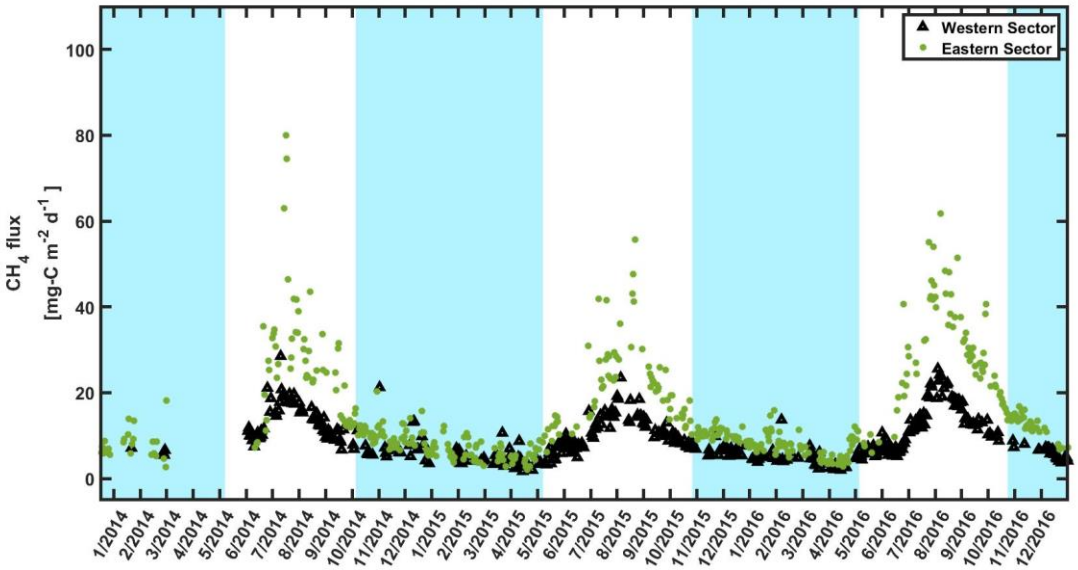

458

459 Figure 5. Time series for non-gap-filled CH_4 daily averaged fluxes for the western sector (green triangles)
460 and the eastern sector (black dots), where the shaded light blue area is frozen period when peat
461 temperature at 10 cm was below 0 °C (see Section 2.8 for a detailed description).

462

463 The middle-day of the peak season of the CH_4 emission was defined as the maximum of the 14-
464 days moving average. Two weeks forward and backward from the middle-day was defined as the
465 peaks season and emissions were estimated for that period in each year. The average emission
466 during the peak seasons was 40 mg-C m^{-2} d^{-1} for the eastern sector and 19 mg-C m^{-2} d^{-1} for the
467 western sector. Detailed emissions for all years are presented in Table 4. The peak season
468 emissions were statistically different from each other ($p < 0.001$). Wintertime fluxes were steadily
469 declining as winter continued and the lowest emissions were observed slightly before the spring
470 thaw. Wintertime average emissions were 9 mg-C m^{-2} d^{-1} for the eastern sector and 6 mg-C m^{-2}
471 d^{-1} for the western sector. Detailed emissions of winter periods are presented in Table 5.

472 Table 4. CH_4 emission during the peak season

	Mean	Standard deviation	The standard error of the mean
	[mg-C m^{-2} d^{-1}]		
2014 E	40.7	17.2	4.3
2015 E	34.4	11.7	3.7
2016 E	45.4	6.7	1.7
2014 W	18.6	3.2	0.8
2015 W	16.1	3.2	1.0
2016 W	20.9	2.6	0.7

473

Table 5. CH_4 emission during the winter period

	Mean	Standard deviation	The standard error of the mean
	[mg-C m^{-2} d^{-1}]		
2014 E	9.0	2.8	0.4
2015 E	8.3	1.7	0.2
2016 E	9.8	2.6	0.3
2014 W	7.2	2.2	0.4
2015 W	5.5	1.4	0.2
2016 W	5.2	3.4	0.4

3.3 Factors controlling the CH_4 fluxes

In the eastern sector, the CH_4 flux correlated best with the peat temperature at 30 cm depth, and in the western sector with the temperature at 10 cm depth. Using temperatures above the level of maximum correlation led to similar hysteresis-like behavior in CH_4 flux - temperature relations as presented by Chang et al. (2020), but using deeper temperatures led to inverse hysteresis compared to shallower temperatures (Figure 6). The correlation matrix (Figure S3) shows the importance of SWC in the CH_4 emissions, while WTL does not correlate significantly with CH_4 flux. Controlling factors were examined before and after temperature normalization of the CH_4 fluxes following Rinne et al. (2018) (Table 6), in order to avoid effect of cross-correlation between explanatory parameters.

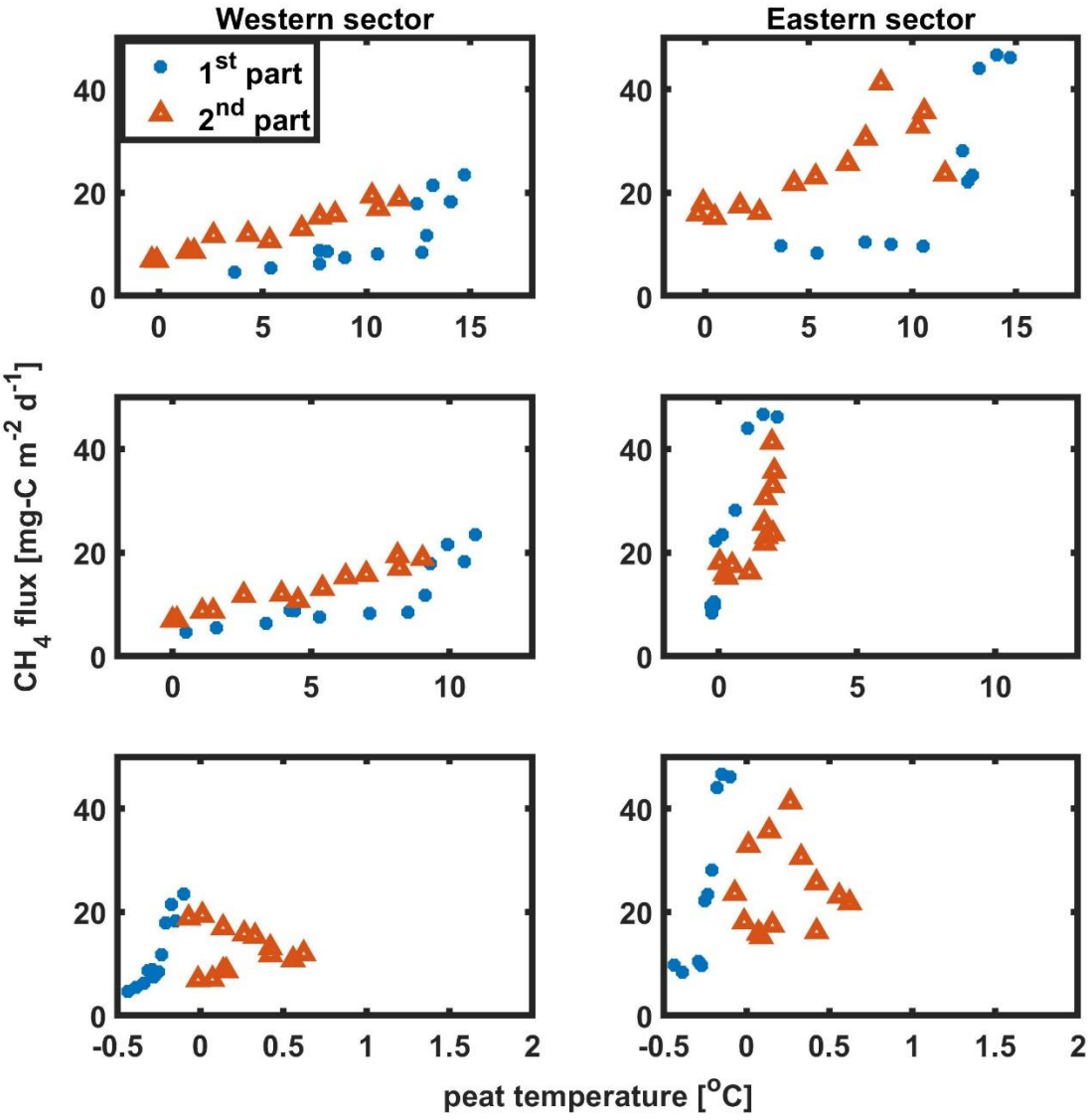

Figure 6. Weekly averages of CH4 fluxes against the surface peat temperature (top panels), the depth with best correlation (middle panels), and the deeper layer (bottom panel). Data were divided into the 1st part of the growing season (blue dots) before the maximum weekly emission, and 2nd part of the growing season (orange triangles) after that.

The result from GLM, showing the variables that contribute to the model, is presented in Table S2. The parameter that was selected first by all models, was peat temperature, at 10 cm depth for the western sector and at 30 cm depth for the eastern sector. For the eastern sector, the GLM algorithm selected SWC as the explanatory factor for CH_4 fluxes during all years as well as for the combined three-year period. The GLMs created for the western sector did not have other explanatory factors besides the peat temperature that were selected in all years. However, two

more explanatory factors, GPP and shortwave incoming radiation, appeared in the three time periods (years 2015 and 2016, and three-years combined) for the western sector.

The eastern sector models had shortwave incoming radiation as the explanatory factor for the year 2015, the year 2016, and combined three-year period. A unique variable for this sector was the vapor pressure deficit, which was used in the models constructed for the years 2016 and combined three-year period.

The year 2014 was characterized by a smaller number of parameters contributing to the models for both sectors compared to other years and combined three-year models. Only peat temperature and SWC were explanatory variables for both sectors in this year. The years 2015 and 2016 and all three years combined have a longer list of parameters.

As the WTL data was available only during a short period of the year, it was not analyzed with the GLM. The WTL measurement in the western sector was not representative of the conditions for most of the sector, this parameter was not used for further analysis from this sector. The WTL was correlated with CH_4 fluxes for the eastern sector.

Based on the chosen explanatory variables it was noticed that the seasonal cycle could be explained by a lower number of parameters than the interannual variation.

Table 6. Summary of controlling factors before and after temperature normalization

Year and ecosystem	R for CH_4 flux	the p-value for CH_4 flux	R for temperature normalized CH_4 flux	the p-value for temperature normalized CH_4 flux
		GPP		
2014 E	0.71	$7x10^{-22}$	-0.03	0.70
2015 E	0.69	$2x10^{-25}$	0.02	0.83
2016 E	0.77	$1x10^{-36}$	0.21	$4x10^{-3}$
2014 W	0.69	$4x10^{-15}$	-0.10	0.36
2015 W	0.73	$6x10^{-29}$	0.05	0.56
2016 W	0.71	$5x10^{-29}$	-0.02	0.76
		WTL		
2014 E	-0.50	2x10-4	1x10-2	0.94
2015 E	-0.20	0.30	-0.20	0.17
2016 E	0.60	4x10-6	-0.30	0.01
		SWC		
2014 E	0.51	$2x10^{-10}$	-0.02	0.79
2015 E	0.51	$1x10^{-12}$	-0.03	0.66
2016 E	0.69	$1x10^{-26}$	0.20	$6x10^{-3}$
2014 W	-0.31	$2x10^{-3}$	-0.37	$2x10^{-4}$
2015 W	0.19	0.02	-0.19	0.02
2016 W	0.22	$3x10^{-3}$	-0.26	$5x10^{-4}$

3.4 Gap-filled annual cycles

Cumulative CH_4 emissions based on different gap-filling methods are presented in Figure 7. All follow a similar annual curve, with a steeper increase in summer, but also relatively high wintertime contribution. Annual, wintertime, and unfrozen period emissions by all gap-filling methods, with their estimated uncertainties, are shown in Figure 8. Emission estimation by each sector and data gap-filled by the different method are presented in Table S3. Average values from all models with their upper and lower limit and wintertime contribution to fluxes are demonstrated in Table 7.

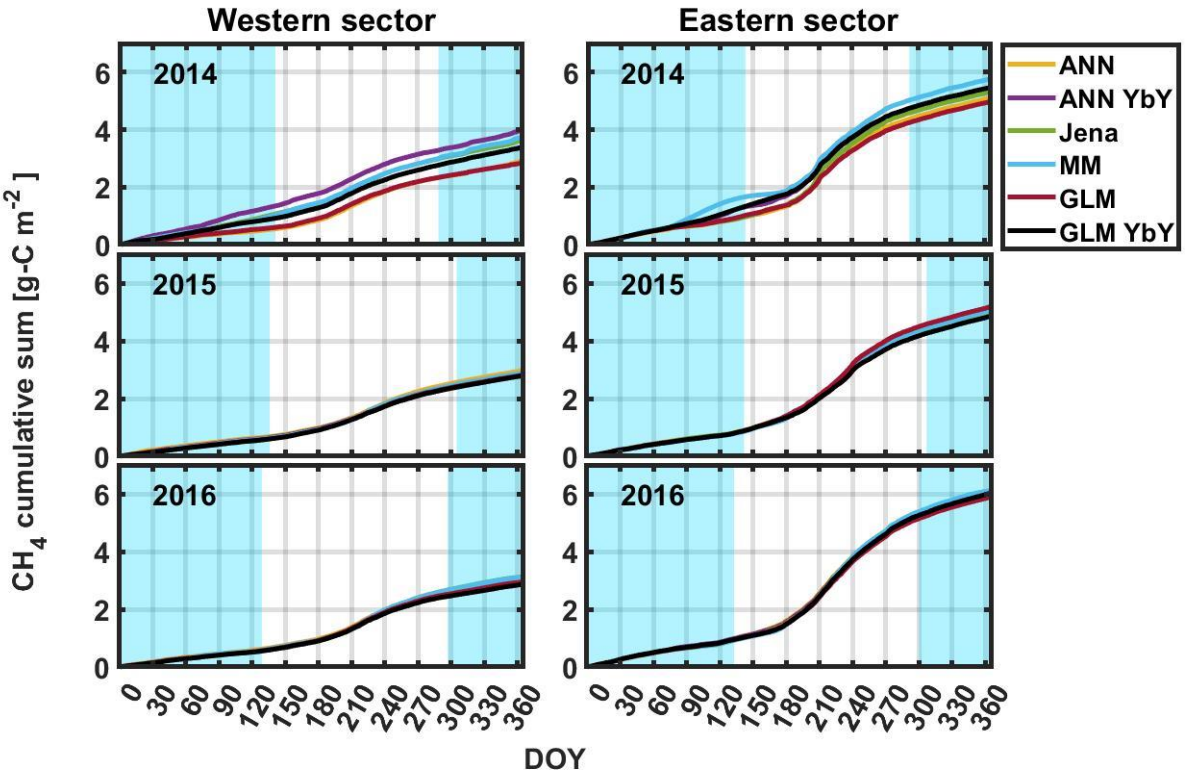

Figure 7. The cumulative sum of CH_4 fluxes for the years 2014-2016 for western and eastern sectors calculated with the different gap-filling methods. ANN - the artificial neural network for all years, ANN YbY - artificial neural network each year separately, Jena - Jena online gap-filling tool, MM - moving mean with 5-day moving window, GLM- the general linear model for all years, GLM YbY - the general linear model for each year separately. The shaded light blue area designates the frozen period when peat temperature at 10 cm was below 0 °C (see Section 2.8 for a detailed description).

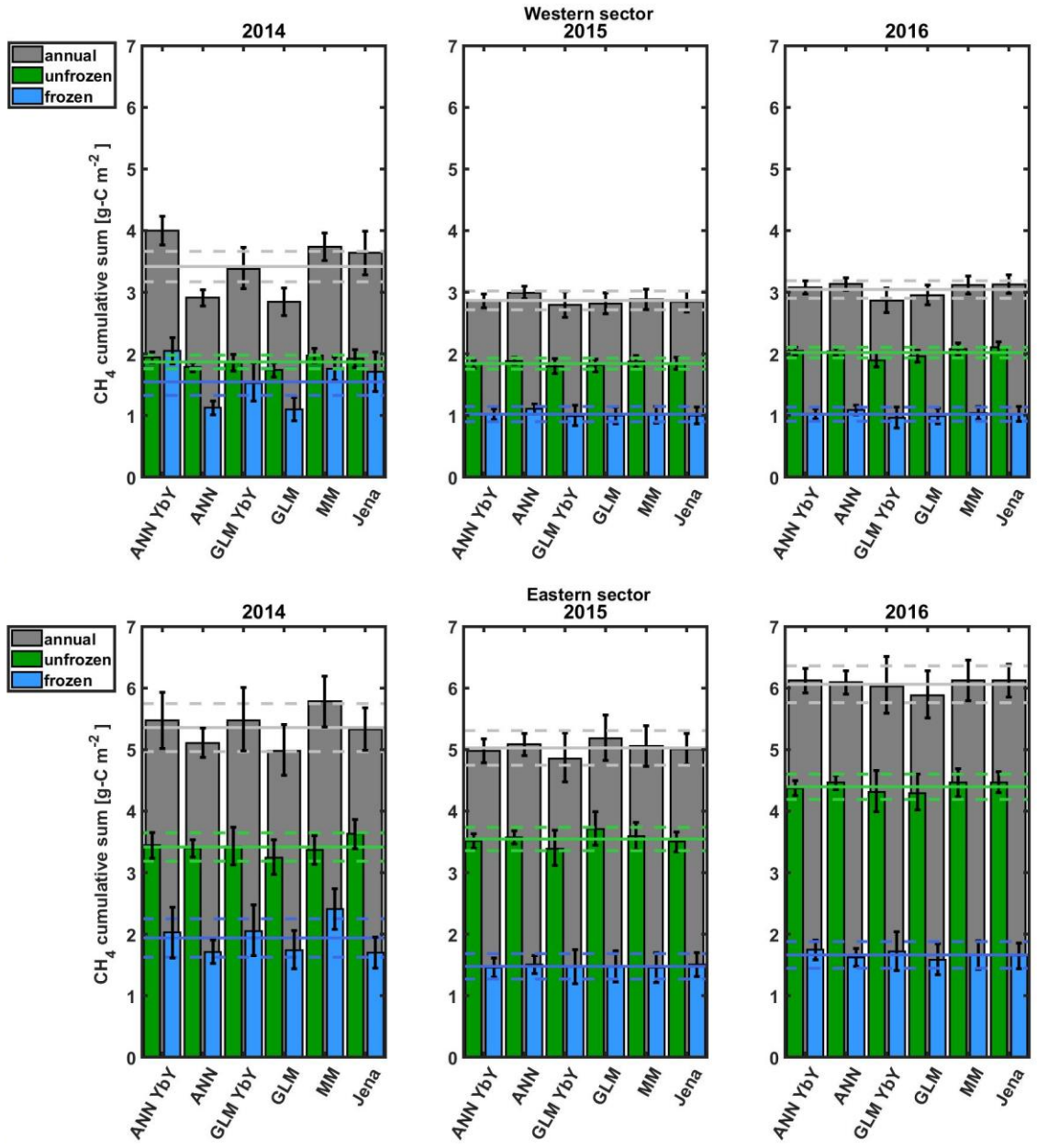

Figure 8. Comparison of cumulative sums of CH_4 fluxes for different gap-filling methods for the western sector (top panel) and eastern sector (bottom panel). ANN - the artificial neural network for all years, ANN YbY - artificial neural network each year separately, Jena - Jena online gap-filling tool, MM - moving mean with 5-day moving window, GLM- the general linear model for all years, GLM YbY - the general linear model for each year separately. Gray bars are for the annual sums, blue bars are for the frozen period sums and green bars are for the unfrozen period (see Section 2.8 for a detailed description). Solid lines are the mean value from all models and dashed lines are for the standard deviation range, with the same colors described above.

As can be seen in Table 3, the year 2014, with a larger difference between annual emissions calculated by different gap-filling methods, had very long gaps that were not present in other years. Also, the uncertainties in annual emission are the largest for the year 2014 for all gap-filling methods, reflecting the gap distribution.

Table 7. Average CH_4 annual emission based on all models with the upper and lower limit and contribution from the winter fluxes.

	Mean	Lower limit	Upper limit	Contribution to wintertime fluxes	Mean	Lower limit	Upper limit	Contribution to wintertime fluxes
	Western sector				Eastern sector			
	g-C m^{-2} a^{-1}			%	g-C m^{-2} a^{-1}			%
2014	3.4	2.8	4.0	45	5.4	5.0	5.8	36
2015	2.8	2.8	3.0	36	5.0	4.9	5.2	29
2016	3.1	2.8	3.1	34	6.1	5.9	6.1	27

Three years' averages of GPP and net ecosystem exchange (NEE) for two sectors are presented in table 8. As comparison, data from lake and tall sedge fen areas at the Stodalen mire complex, where permafrost was completely thawed, are also presented (Jammet et al., 2017). The fen has the highest percentage of carbon emitted as CH_4, as compared to the annual CO_2 uptake. The eastern and the western sectors emitted less of the assimilated carbon as CH_4 compared to the completely thawed area. The uptake of carbon as CO_2 was also largest at the fen.

Table 8. Average annual GPP, NEE and CH_4 emission from western and eastern sector in comparison to fen.

	GPP	NEE	CH_4	CH_4/GPP	CH_4/NEE
	g-C m^{-2} a^{-1}	g-C m^{-2} a^{-1}	g-C m^{-2} a^{-1}	%	%
Western sector	225	-28.9	3.1	1.4	19.6
Eastern Sector	257	-42.0	5.5	2.2	14.0
Fen (Jammet et al. 2017)	N.A.	-66.3	21.2	N.A.	32.0

The 3 years' annual average CH_4 emissions of palsa and thawing surfaces, as calculated by Eq. (1) and (2), are presented in Table 9. For comparison average annual emissions from other major surface types, measured by EC technique, are shown as well. The emission from the tall

graminoid fen, a third mire type common at Stordalen Mire, has been previously measured using the EC method by Jackowicz-Korczyński et al. (2010) and Jammet et al. (2017). In addition to these, the mire complex includes shallow lakes. Their annual CH_4 emission has been measured by EC method by Jammet et al., (2017).

Table 9. Annual CH_4 emission from different components of the Stordalen Mire complex from EC studies.

type of wetland	Annual emission [g-C m^{-2} a^{-1}]	References
palsa plateau surface	2.7 ± 0.5	this study
thawing wet surface	8.2 ± 1.5	this study
thawed fen	15.8 ± 1.6	Jackowicz-Korczyński et al. 2010
thawed fen	21.2 ± 1.3	Jammet et al. 2017
shallow lake	4.9 ± 0.6	Jammet et al. 2017

4 Discussion

4.1 Differences in controlling factors

According to the GLM, peat temperature and GPP were typically the first parameters selected by the algorithm to explain CH_4 fluxes. In the eastern sector, the CH_4 flux correlated best with the peat temperature at 30 cm depth, and in the western sector with the peat temperature at 10 cm depth. Temperature as a controlling factor of CH_4 emission has been reported in many wetlands studies (Christensen et al. 2003, Jackowicz-Korczyński et al. 2010, Bansal et al. 2016, Pugh et al. 2017, Rinne et al. 2007; 2018), in line with our findings. The correlation of CH_4 fluxes with the temperature at 5 cm depth was also higher than for 30 cm in the western sector. As the peat in the palsa is frozen at 30 cm depth for most of the growing season, the correlation between CH_4 fluxes and temperature at these depths is lower. Temperature correlation for the upper part, 2 cm, and 5 cm depth, shows a similar level of correlation as presented by Jackowicz-Korczyński et al. (2010). As they did not analyze correlation with the temperature at deeper peat, we cannot compare these results. The hysteresis-like behavior of the CH_4 flux – temperature relation is similar to that observed by Chang et al. (2020) when using temperatures measured above the depth of maximum correlation, but inversed when using temperatures measured at deeper depths (Figure 6). This is in line with at least part of the hysteresis-like behavior to be due to the lag of seasonal temperature wave at the depth of CH_4 production compared to the timing of the temperature wave at shallower depth or air temperature.

GPP was indicated as a controlling factor for CH_4 emission from a boreal fen ecosystem by Rinne et al. (2018). In our study, the correlation matrix shows a significant correlation between daily average GPP and CH_4 flux at both sectors (Table S3). To disentangle the confounding effects of temperature and GPP, we used temperature-normalized CH_4 fluxes following Rinne et al. (2018) which revealed that the correlation between GPP and temperature-normalized CH_4 flux was not significant in most years (Table 6). Only the data from the eastern sector in the year 2016 shows a significant correlation. Thus, it seems hard to disentangle the effects of temperature and GPP

on CH_4 fluxes using this data set. As our data set consists of only three years, the analysis of interannual variations would not be a robust approach either.

Solar shortwave incoming radiation was selected as a controlling variable by 6 of 8 GLM models (Table S3). This parameter has an indirect effect on CH_4 production via photosynthesis and subsequent substrate production. The maximum emission of CH_4 occurs later in the year than maximum radiation. This may be due to the CH_4 emission depending on the deeper peat temperature or seasonal cycle of available substrates, lagging behind the annual cycle of radiation (e.g. Rinne et al., 2018; Chang et al., 2020). The negative contribution of shortwave radiation in GLM can be due to the slight diel cycle of CH4 emission, with lowest values at daytime. Mechanistically we can think that the solar irradiance will heat the top of the peat layer, thus leading to increased methanotrophy at daytime (see discussion above on diel cycle). This can lead to situation where the methanotrophy is higher in sunny days with warm surface and lower in cloudy days. The role of photosynthesis for the substrate supply of methanogenesis is likely to act in the seasonal time scale, where its effect can be masked by the strong correlation between peat temperature and CH4 emission. The highest correlation of CH_4 flux and radiation was observed in 2014, but GLM did not select radiation as an explanatory factor for this year. Other years and the whole period show a much lower correlation.
CH_4 fluxes from wetlands have been shown to depend on WTL in many studies (e.g. Bubier et al., 2005; Turetsky et al., 2014; Rinne et al., 2020). However, in a number of studies, the CH_4 fluxes have shown to be relatively insensitive to the small variation, without strong extreme conditions, in the WTL (Rinne et al. 2007, 2018, Jackowicz-Korczyński et al. 2010). In the eastern sector, CH_4 flux and WTL were correlated for the years 2014 and 2016. However, after normalization of CH_4 fluxes with their temperature dependence following Rinne et al., (2007), correlations were mostly not significant (Table 6). This is similar to conclusions drawn by e.g. Rinne et al. (2007, 2018) and Jackowicz-Korczyński et al. (2010).

Instead of WTL, we used SWC as a possible controlling factor for the CH_4 emission from the western sector. Sturtevant et al. (2012) also reported SWC as a controlling factor in autumn. SWC shows correlation on a significant level before and after normalization for three years for the western sectors (Table 6).

The GLM algorithm selected SWC as one of the explaining factors while constructing the GLM for the eastern sector for the whole measurement season. It was chosen by models built for three years together and each year separately. R and p-value are presented in Table 6. A reduction of R and increase in p-value after temperature normalization is similar to previous parameters. The correlation of CH_4 emission with SWC stays on a significant level only in the year 2016.

4.2 Gap-filling methods

In general, the gap-filled annual CH_4 emissions were within their estimated uncertainty from each other, apart from the year 2014. The results of different gap-filling methods were affected by the

637 different gap distributions and lengths in different years and the two wind sectors. Thus, below
638 we discuss the method performance separately for the year 2014 and the two other years.

639 The dataset from the eastern sector was gap-filled with higher confidence than for the western
640 sector in 2014. The data from the eastern sector contains fewer very long gaps - more than 30
641 days, and fewer long gaps - more than 8 but less than 30 days. The method which was most
642 affected by long gaps was the moving mean approach, indicating that this method should not be
643 used for data sets with very long gaps. The ANN and the GLM gap-filling methods based on the
644 whole data set estimated lower annual emission than mean emission from all methods. For two
645 years without very long gaps (2015 and 2016), the Jena gap-filling tool was assumed as a baseline
646 method, as it is commonly used for gap-filling of especially CO_2 fluxes. It is independent of the
647 user choices, as the ecosystem variables required have been chosen by the developers. However,
648 as this gap-filling tool has been developed for CO_2, not all the variables are necessarily relevant
649 for the gap-filling of the CH_4 time series. Furthermore, the Jena gap-filling tool works in a half-
650 hourly resolution to resolve the diel variation in CO_2 fluxes. As the sub-daily variation in CH_4 fluxes
651 is largely random noise in many mires (Rinne et al., 2007; 2018; Jackowicz-Korczyński et al., 2010),
652 developing a similar tool working at daily time step for CH_4, and with tailored parameter set for
653 CH_4, would be useful.

654 The moving mean approach resulted in annual fluxes within the range of standard deviation from
655 the Jena gap-filling tool. Daily values probably vary less than values obtained by the Jena tool
656 because moving means smooth the data. Additional advantages of this method are low input
657 requirements, as no auxiliary data is needed.

658 Annual estimates of CH_4 emission, based on the gap-filling with algorithms developed for the
659 whole data set, could be biased when the ecosystem is changing fast between the years and
660 functional dependencies on environmental parameters change. The annual CH_4 emissions by
661 ANN, based on the whole data set and based on one-year data, agree within the standard
662 deviation for the years 2015 and 2016. Both of them are also in agreement with the baseline
663 method within the standard deviation.

664 The feasibility of GLM is similar to ANN. The GLM model built on the whole dataset is sensitive to
665 rapid changes in ecosystem functioning and the number of gaps each year. A year with more gaps
666 has a lower influence on the model, similarly to the ANN. However, annual CH_4 emissions derived
667 using GLMs, based on each year separately or the whole dataset, agree with one another and
668 with baseline model within the standard deviation. GLM required more preparation than ANN.
669 Before developing the GLMs, highly correlated parameters need to be determined. The selection
670 of relevant variables is crucial for the correct performance of that algorithm and the selection
671 influences model output and model uncertainties.

672 According to the analysis with artificial gaps, the 35-day artificial gap did not change annual sums
673 significantly for any gap-filling method. The 80-day artificial gap created a significant difference
674 for the eastern sector in the year 2015 for ANN YbY and 2016 for ANN (Figure S7). The unfrozen

period did not show significant differences between annual sums for any method. The wintertime period was statistically different for the year 2015 for ANN YbY. The results with the 80-day gap had higher uncertainties than the results with a 35-day gap. The existence of gaps in the winter period did not have a significant impact on the unfrozen period fluxes.

All presented methods show similar CH_4 emissions. Choosing one of them as the most appropriate is not obvious, because all of them show both advantages and disadvantages. The method that required the least amount of preparation before use and that was thus the fastest to apply is the moving mean. It can be used for short gaps with good results and does not need additional measured variables to work properly. The ANN method require less preparation than other methods i.e. following the template or choosing the correct variables and it gives similar results. It could be recommended as a gap-filling method suitable for different sites due to unique construction of the ANN for each place.

4.3 Winter fluxes

The winter fluxes from both sectors were positive, which is in line with observations by e.g. Rinne et al. (2007, 2018, 2020) and Jammet et al. (2017) of wintertime CH_4 emissions from frozen northern mires. Winter emission and potential spring thaw bursts of CH_4 can be mechanistically connected (Taylor et al. 2018), while degassing of CH_4 during the winter is likely to lead to smaller or no thaw bursts of CH_4. Thus, EC studies on the seasonal cycle of CH_4 emissions from other seasonally frozen mire ecosystems have shown minor or no thaw emission pulse (Rinne et al., 2007; 2018; Mikhaylov et al. 2015). On the contrary, many studies show spring-thaw emissions from shallow lakes (Raz-Yaseef et al. 2017, Jammet et al. 2015, 2017). In lakes, winter fluxes can be blocked by a solid ice layer leading to the build-up of CH_4 below ice during the frozen period (Jammet et al. 2017). On mires, however, the ice cover is not as solid as in lakes, but more porous due to peat and plants within the ice. Therefore, the diffusion during the frozen period is considerably faster than through lake ice. Furthermore, Song et al. (2012) showed that spring burst events could occur at a very small scale and very short in duration (e.g. 2 hours). Small-scale events show a lower influence on EC measurements because the method averages over a larger area. Moreover, if the small-scale short-duration event does not happen in the EC footprint e.g. due to wind direction, it will be missed.

We did not observe an autumn freeze-in burst in our data from either sector at Stordalen Mire. These events have been observed at a High-Arctic tundra site (Mastepanov et al. 2013) though not every year. Mastepanov et al. (2008) suggested that freeze-in bursts of CH_4 could be observed only in the Arctic with continuous permafrost and not in a subarctic area with discontinuous or sporadic permafrost. The phenomenon is assumed to be connected to the expansion of water upon freezing, causing air bubbles to be mechanically pushed out of the freezing soil.

4.4 Different permafrost status and CH_4 emissions

Stordalen Mire is a complex mire system, with at least three different main wetlands surface types and different permafrost status within a distance of a few hundred meters. The permafrost palsa development and thaw depend both on temperature and snow cover and it is partly self-regulating via the effect of microtopography on local snow depth (Johansson et al. 2006). Due to the recently increasing temperatures, the thaw processes are currently likely to dominate over palsa growth. CH_4 emission from the different microforms in mire systems depends on the hydrological and nutrient status and temperature which affect e.g. plant and microbial communities.

The carbon emitted as the CH_4 fluxes from the eastern and western sector is on similar level to the Siikaneva fen (Rinne et al. 2018). In comparison to the other fen sites reviewed by Rinne et al. (2018), the ratio of CH_4 to NEE at Stordalen Mire is higher. The reason behind this could be the shorter growing season and thus lower CO_2 fluxes.

The average annual CH_4 emissions from different surfaces (Table 9) shows that the palsas have the lowest annual CH_4 emissions, followed by a lake. The fully thawed fen, dominated by tall graminoids, has very high annual CH_4 emissions and the highest of the mire complex, surpassing e.g. many boreal poor fens (Nilsson et al., 2008; Rinne et al., 2018). The thawing surfaces common in the eastern footprint of the tower have annual CH_4 emissions between palsas and tall sedge fen. The three surface types studied here and previously by Jackowicz-Korczyński et al. (2010) and Jammet et al., (2017) can be seen as forming a thaw gradient in this subarctic environment. The globally rising temperature is likely to lead to continuing permafrost thaw in this kind of ecosystem and increased CH_4 emissions.

5 Conclusion

At our study site, eddy covariance fluxes were measured for two different subarctic mire areas, one dominated by palsa plateaus and the other a mixture of palsas and thawing wet surfaces. The measurements revealed clear differences in their annual CH_4 emissions, with the area dominated by palsas emitting less. The annual emission from a thawing surface (8.2 g-C m^{-2} a^{-1}) was nearly three times higher than from palsa surfaces (2.7 g-C m^{-2} a^{-1}) but only half of the emission previously reported from fully thawed tall graminoid fen. Areas measured in this study had similar seasonal cycles of emission, with maxima appearing in August and lower but significant fluxes in winter. The seasonal cycles were furthermore characterized by a fast increase in spring (average 0.21 mg-C m^{-2} d^{-2} for the western sector and 0.68 mg-C m^{-2} d^{-2} for the eastern sector) and a less rapid decrease in fall (average -0.16 mg-C m^{-2} d^{-2} for the western sector and -0.37 mg-C m^{-2} d^{-2} for the eastern sector), without any obvious burst events during spring thaw or autumn freeze-in. The wintertime period (from January to mid-May and from late-October to December) contributed with 27 % - 45 % to the annual emission.

According to the correlation matrix and GLM analysis, CH_4 emissions from the western and eastern sectors were partly controlled by different factors. As in most studies on CH_4 emission from wetlands, peat temperature was the most important factor explaining the emission. The relation of CH_4 flux with peat temperature at shallower depths showed similar hysteresis-like behavior than observed by Chang et al. (2020), but inverse behavior with temperature at deeper peat. We showed that the existence and direction of hysteresis-like behavior can depend on which depth the temperature is measured.

The correlation of CH_4 emission and WTL in the eastern sector was not significant, but in the western sector, the SWC did appear to control the emission.

The estimation of annual CH_4 emission was based on gap-filling with four different methods. All methods resulted in similar annual fluxes, especially for the two years with just relatively short gaps (less than 8 days). The performance of the methods was also dependent on the gap distribution. Long gaps (more than 8 days) were the most problematic to be reconstructed by any of the methods. The average annual emission from the western sector was 3.1 g-C m^{-2} a^{-1} and from the eastern sector was 5.5 g-C m^{-2} a^{-1}. Both were substantially lower than those obtained from a tall graminoid fen at the same mire system.

Based on the presented results further studies should focus on winter fluxes, which are important in the northern, low emissions wetlands with discontinuous permafrost. There is still a lack in understanding the processes behind those emissions. Also, the origin of wintertime CH_4 emission is somewhat unknown. On the one hand, CH_4 can be produced during the winter period, on the other hand CH_4 can also be produced during the growing season, remain stored in the peat and then be slowly released during the frozen period. These processes could possibly explain the hysteresis-like behavior of CH_4 emissions.

Data and code availability

http://doi.org/10.5281/zenodo.4640164s

Author contribution

P.Ł., J.H. T.F., P.C. and J.R. analysed and interpreted the data. P.Ł., J.H., P.C., J.R. wrote the manuscript. T.F., P.C. and, N.R. designed the measurements. N.K. was responsible for the footprint calculation and its interpretation. P.-O.O. and L.E. were responsible for interpreting UAV data. A. P. supported with the water table level data.

Competing interests

The authors declare that they have no conflict of interest

Acknowledgements

This study is funded by MEthane goes Mobile: MEasurement and MOdeling (MEMO2) project from the European Union's Horizon 2020 research and innovation programme under the Marie Sklodowska-Curie grant agreement No 722479. Data was provided by the Abisko Scientific Research Station (ANS) and Swedish Infrastructure for Ecosystem Sciences (SITES, co-financed by the Swedish Research Council) hosting the Stordalen site, part of the ICOS-Sweden network which was co-financed by the Swedish Research Council (grant-no. 2015-06020, 2019-00205). Image collection using the UAV was done by Matthias Siewert in collaboration with the SITES Spectral project.

References

Åkerman, H. J. and Johansson, M.: Thawing permafrost and thicker active layers in sub-arctic Sweden, Permafr. Periglac. Process., 19, 279–292, https://doi.org/10.1002/ppp.626, 2008.

Bansal, S., Tangen, B., and Finocchiaro, R.: Temperature and Hydrology Affect Methane Emissions from Prairie Pothole Wetlands, 36, 371–381, https://doi.org/10.1007/s13157-016-0826-8, 2016.

Brantley, H. L., Thoma, E. D., Squier, W. C., Guven, B. B., and Lyon, D.: Assessment of Methane Emissions from Oil and Gas Production Pads using Mobile Measurements, Environ. Sci. Technol., 48, 14508–14515, https://doi.org/10.1021/es503070q, 2014.

Bubier, J., Moore, T., Savage, K., and Crill, P.: A comparison of methane flux in a boreal landscape between a dry and a wet year, Global Biogeochem. Cycles, 19, https://doi.org/10.1029/2004GB002351, 2005.

Budishchev, A., Mi, Y., van Huissteden, J., Belelli-Marchesini, L., Schaepman-Strub, G., Parmentier, F. J. W., Fratini, G., Gallagher, A., Maximov, T. C., and Dolman, A. J.: Evaluation of a plot-scale methane emission model using eddy covariance observations and footprint modelling, 11, 4651–4664, https://doi.org/10.5194/bg-11-4651-2014, 2014.

Callaghan, T. V, Bergholm, F., Christensen, T. R., Jonasson, C., Kokfelt, U., and Johansson, M.: A new climate era in the sub-Arctic: Accelerating climate changes and multiple impacts, Geophys. Res. Lett., 37, https://doi.org/10.1029/2009GL042064, 2010.

Callaghan, T. V, Jonasson, C., Thierfelder, T., Yang, Z., Hedenås, H., Johansson, M., Molau, U., Van Bogaert, R., Michelsen, A., Olofsson, J., Gwynn-Jones, D., Bokhorst, S., Phoenix, G., Bjerke, J. W., Tømmervik, H., Christensen, T. R., Hanna, E., Koller, E. K., and Sloan, V. L.: Ecosystem change and stability over multiple decades in the Swedish subarctic: complex processes and multiple drivers, Philos. Trans. R. Soc. B Biol. Sci., 368, 20120488, https://doi.org/10.1098/rstb.2012.0488, 2013.

819 Chang, K.-Y., Riley, W. J., Crill, P. M., Grant, R. F., and Saleska, S. R.: Hysteretic temperature
820 sensitivity of wetland CH4 fluxes explained by substrate availability and microbial activity, 17,
821 5849–5860, https://doi.org/10.5194/bg-17-5849-2020, 2020.

822 Christensen, T. R., Friborg, T., Sommerkorn, M., Kaplan, J., Illeris, L., Soegaard, H., Nordstroem,
823 C., and Jonasson, S.: Trace gas exchange in a high-Arctic valley: 1. Variationsin CO2 and CH4 Flux
824 between tundra vegetation types, Global Biogeochem. Cycles, 14, 701–713,
825 https://doi.org/10.1029/1999GB001134, 2000.

826 Christensen, T. R., Ekberg, A., Ström, L., Mastepanov, M., Panikov, N., Öquist, M., Svensson, B.
827 H., Nykänen, H., Martikainen, P. J., and Oskarsson, H.: Factors controlling large scale variations
828 in methane emissions from wetlands, Geophys. Res. Lett., 30,
829 https://doi.org/10.1029/2002GL016848, 2003.

830 Deng, J., Li, C., Frolking, S., Zhang, Y., Bäckstrand, K., and Crill, P.: Assessing effects of
831 permafrost thaw on C fluxes based on multiyear modeling across a permafrost thaw gradient at
832 Stordalen, Sweden, 11, 4753–4770, https://doi.org/10.5194/bg-11-4753-2014, 2014.

833 Dengel, S., Zona, D., Sachs, T., Aurela, M., Jammet, M., Parmentier, F. J. W., Oechel, W., and
834 Vesala, T.: Testing the applicability of neural networks as a gap-filling method using CH4 flux
835 data from high latitude wetlands, 10, 8185–8200, https://doi.org/10.5194/bg-10-8185-2013,
836 2013.

837 Dlugokencky, E. J., Nisbet, E. G., Fisher, R., and Lowry, D.: Global atmospheric methane: budget,
838 changes and dangers, Philos. Trans. R. Soc. A Math. Phys. Eng. Sci., 369, 2058–2072,
839 https://doi.org/10.1098/rsta.2010.0341, 2011.

840 Dobson 1945-, A. J.: An introduction to generalized linear models / Annette J. Dobson,
841 Chapman & Hall/CRC, Boca Raton, 2002.

842 Dragomir, C. M., Klaassen, W., Voiculescu, M., Georgescu, L. P., and van der Laan, S.: Estimating
843 Annual CO2 Flux for Lutjewad Station Using Three Different Gap-Filling Techniques, Sci. World
844 J., 2012, 842893, https://doi.org/10.1100/2012/842893, 2012.

845 Edie, R., Robertson, A. M., Field, R. A., Soltis, J., Snare, D. A., Zimmerle, D., Bell, C. S., Vaughn, T.
846 L., and Murphy, S. M.: Constraining the Accuracy of Flux Estimates Using OTM 33A, 2019, 1–27,
847 https://doi.org/10.5194/amt-2019-306, 2019.

848 Falge, E., Baldocchi, D., Olson, R., Anthoni, P., Aubinet, M., Bernhofer, C., Burba, G., Ceulemans,
849 R., Clement, R., Dolman, H., Granier, A., Gross, P., Grünwald, T., Hollinger, D., Jensen, N.-O.,
850 Katul, G., Keronen, P., Kowalski, A., Lai, C. T., Law, B. E., Meyers, T., Moncrieff, J., Moors, E.,
851 Munger, J. W., Pilegaard, K., Rannik, Ü., Rebmann, C., Suyker, A., Tenhunen, J., Tu, K., Verma, S.,
852 Vesala, T., Wilson, K., and Wofsy, S.: Gap filling strategies for defensible annual sums of net
853 ecosystem exchange, Agric. For. Meteorol., 107, 43–69, https://doi.org/10.1016/S0168-
854 1923(00)00225-2, 2001a.

855 Falge, E., Baldocchi, D., Olson, R., Anthoni, P., Aubinet, M., Bernhofer, C., Burba, G., Ceulemans,
856 R., Clement, R., Dolman, H. (A. J. ., Granier, A., Gross, P., Grünwald, T., Hollinger, D., Jensen, N.

857 O., Katul, G., Keronen, P., Kowalski, A., Lai, C.-T., and Tu, K.: Gap filling strategies for long term
858 energy flux data sets, Agric. For. Meteorol. 107 71-77, 2001b.

859 Fisher, R. E., France, J. L., Lowry, D., Lanoisellé, M., Brownlow, R., Pyle, J. A., Cain, M., Warwick,
860 N., Skiba, U. M., Drewer, J., Dinsmore, K. J., Leeson, S. R., Bauguitte, S. J.-B., Wellpott, A.,
861 O'Shea, S. J., Allen, G., Gallagher, M. W., Pitt, J., Percival, C. J., Bower, K., George, C., Hayman, G.
862 D., Aalto, T., Lohila, A., Aurela, M., Laurila, T., Crill, P. M., McCalley, C. K., and Nisbet, E. G.:
863 Measurement of the 13C isotopic signature of methane emissions from northern European
864 wetlands, Global Biogeochem. Cycles, 31, 605–623, https://doi.org/10.1002/2016GB005504,
865 2017.

866 Friborg, T., Christensen, T. R., and Søgaard, H.: Rapid response of greenhouse gas emission to
867 early spring thaw in a subarctic mire as shown by micrometeorological techniques, Geophys.
868 Res. Lett., 24, 3061–3064, https://doi.org/doi:10.1029/97GL03024, 1997.

869 Gao, X., Adam Schlosser, C., Sokolov, A., Anthony, K. W., Zhuang, Q., and Kicklighter, D.:
870 Permafrost degradation and methane: low risk of biogeochemical climate-warming feedback,
871 Environ. Res. Lett., 8, 35014, https://doi.org/10.1088/1748-9326/8/3/035014, 2013.

872 Gioli, B., Miglietta, F., Martino, B., Hutjes, R., Dolman, H. (A. J. ., Lindroth, A., Schumacher, M.,
873 Sanz-Sanchez, M.-J., Manca, G., Peressotti, A., and Dumas, E.: Comparison between tower and
874 aircraft-based eddy covariance fluxes in five European regions, Agric. For. Meteorol., 127, 1–16,
875 https://doi.org/10.1016/j.agrformet.2004.08.004, 2004.

876 Godin, A., McLaughlin, J. W., Webster, K. L., Packalen, M., and Basiliko, N.: Methane and
877 methanogen community dynamics across a boreal peatland nutrient gradient, Soil Biol.
878 Biochem., 48, 96–105, https://doi.org/https://doi.org/10.1016/j.soilbio.2012.01.018, 2012.

879 Harenda, K., Lamentowicz, M., Samson, M., and Chojnicki, B.: The Role of Peatlands and Their
880 Carbon Storage Function in the Context of Climate Change, in: GeoPlanet: Earth and Planetary
881 Sciences, 169–187, https://doi.org/10.1007/978-3-319-71788-3_12, 2018.

882 Hommeltenberg, J., Schmid, H. P., Drösler, M., and Werle, P.: Can a bog drained for forestry be
883 a stronger carbon sink than a natural bog forest?, 11, 3477–3493, https://doi.org/10.5194/bg-
884 11-3477-2014, 2014.

885 Intergovernmental Panel on Climate Change (Ed.): Anthropogenic and Natural Radiative
886 Forcing, in: Climate Change 2013 – The Physical Science Basis: Working Group I Contribution to
887 the Fifth Assessment Report of the Intergovernmental Panel on Climate Change, Cambridge
888 University Press, Cambridge, 659–740, https://doi.org/DOI: 10.1017/CBO9781107415324.018,
889 2014.

890 Ise, T., Dunn, A. L., Wofsy, S. C., and Moorcroft, P. R.: High sensitivity of peat decomposition to
891 climate change through water-table feedback, Nat. Geosci., 1, 763–766,
892 https://doi.org/10.1038/ngeo331, 2008.

893 Jackowicz-Korczyński, M., Christensen, T. R., Bäckstrand, K., Crill, P., Friborg, T., Mastepanov,
894 M., and Ström, L.: Annual cycle of methane emission from a subarctic peatland, J. Geophys. Res.

Biogeosciences, 115, https://doi.org/10.1029/2008JG000913, 2010.

Jammet, M., Crill, P., Dengel, S., and Friborg, T.: Large methane emissions from a subarctic lake during spring thaw: Mechanisms and landscape significance, J. Geophys. Res. Biogeosciences, 120, 2289–2305, https://doi.org/10.1002/2015JG003137, 2015.

Jammet, M., Dengel, S., Kettner, E., Parmentier, F.-J. W., Wik, M., Crill, P., and Friborg, T.: Year-round CH4 and CO2 flux dynamics in two contrasting freshwater ecosystems of the subarctic, 14, 5189–5216, https://doi.org/10.5194/bg-14-5189-2017, 2017.

JOHANSSON, T., MALMER, N., CRILL, P. M., FRIBORG, T., ÅKERMAN, J. H., MASTEPANOV, M., and CHRISTENSEN, T. R.: Decadal vegetation changes in a northern peatland, greenhouse gas fluxes and net radiative forcing, Glob. Chang. Biol., 12, 2352–2369, https://doi.org/10.1111/j.1365-2486.2006.01267.x, 2006.

Kirschke, S., Bousquet, P., Ciais, P., Saunois, M., Canadell, J. G., Dlugokencky, E. J., Bergamaschi, P., Bergmann, D., Blake, D. R., Bruhwiler, L., Cameron-Smith, P., Castaldi, S., Chevallier, F., Feng, L., Fraser, A., Heimann, M., Hodson, E. L., Houweling, S., Josse, B., Fraser, P. J., Krummel, P. B., Lamarque, J.-F., Langenfelds, R. L., Le Quéré, C., Naik, V., O'Doherty, S., Palmer, P. I., Pison, I., Plummer, D., Poulter, B., Prinn, R. G., Rigby, M., Ringeval, B., Santini, M., Schmidt, M., Shindell, D. T., Simpson, I. J., Spahni, R., Steele, L. P., Strode, S. A., Sudo, K., Szopa, S., van der Werf, G. R., Voulgarakis, A., van Weele, M., Weiss, R. F., Williams, J. E., and Zeng, G.: Three decades of global methane sources and sinks, Nat. Geosci., 6, 813–823, https://doi.org/10.1038/ngeo1955, 2013.

Kljun, N., Calanca, P., Rotach, M. W., and Schmid, H. P.: A simple two-dimensional parameterisation for Flux Footprint Prediction (FFP), Geosci. Model Dev., 8, 3695–3713, https://doi.org/10.5194/gmd-8-3695-2015, 2015.

Knox, S. H., Matthes, J. H., Sturtevant, C., Oikawa, P. Y., Verfaillie, J., and Baldocchi, D.: Biophysical controls on interannual variability in ecosystem-scale CO2 and CH4 exchange in a California rice paddy, J. Geophys. Res. Biogeosciences, 121, 978–1001, https://doi.org/10.1002/2015JG003247, 2016.

Knox, S. H., Windham-Myers, L., Anderson, F., Sturtevant, C., and Bergamaschi, B.: Direct and Indirect Effects of Tides on Ecosystem-Scale CO2 Exchange in a Brackish Tidal Marsh in Northern California, J. Geophys. Res. Biogeosciences, 123, 787–806, https://doi.org/10.1002/2017JG004048, 2018.

Kowalska, N., Chojnicki, B., Rinne, J., Haapanala, S., Siedlecki, P., Urbaniak, M., Juszczak, R., and Olejnik, J.: Measurements of methane emission from a temperate wetland by eddy covariance method, Int. Agrophysics, 27, 283–290, https://doi.org/10.2478/v10247-012-0096-5, 2013.

LEVENBERG, K.: A METHOD FOR THE SOLUTION OF CERTAIN NON-LINEAR PROBLEMS IN LEAST SQUARES, Q. Appl. Math., 2, 164–168, 1944.

Li, T., Raivonen, M., Alekseychik, P., Aurela, M., Lohila, A., Zheng, X., Zhang, Q., Wang, G., Mammarella, I., Rinne, J., Yu, L., Xie, B., Vesala, T., and Zhang, W.: Importance of vegetation

933 classes in modeling CH4 emissions from boreal and subarctic wetlands in Finland, Sci. Total
934 Environ., 572, 1111–1122, https://doi.org/https://doi.org/10.1016/j.scitotenv.2016.08.020,
935 2016.

936 LUNDEGÅRDH, H.: CARBON DIOXIDE EVOLUTION OF SOIL AND CROP GROWTH, Soil Sci., 23,
937 1927.

938 Malmer, N., Johansson, T., Olsrud, M., and Christensen, T. R.: Vegetation, climatic changes and
939 net carbon sequestration in a North-Scandinavian subarctic mire over 30 years, Glob. Chang.
940 Biol., 11, 1895–1909, https://doi.org/10.1111/j.1365-2486.2005.01042.x, 2005.

941 Marquardt, D. W.: An Algorithm for Least-Squares Estimation of Nonlinear Parameters, J. Soc.
942 Ind. Appl. Math., 11, 431–441, 1963.

943 Mastepanov, M., Sigsgaard, C., Dlugokencky, E. J., Houweling, S., Ström, L., Tamstorf, M. P., and
944 Christensen, T. R.: Large tundra methane burst during onset of freezing, Nature, 456, 628–630,
945 https://doi.org/10.1038/nature07464, 2008.

946 Mastepanov, M., Sigsgaard, C., Tagesson, T., Ström, L., Tamstorf, M. P., Lund, M., and
947 Christensen, T. R.: Revisiting factors controlling methane emissions from high-Arctic tundra, 10,
948 5139–5158, https://doi.org/10.5194/bg-10-5139-2013, 2013.

949 Mauder, M. and Foken, T.: Documentation and Instruction Manual of the Eddy Covariance
950 Software Package TK2, Arbeitsergebnisse, Univ. Bayreuth, Abteilung Mikrometeorologie, ISSN
951 1614-8916, 46, https://doi.org/10.5194/bg-5-451-2008, 2011.

952 McCalley, C. K., Woodcroft, B. J., Hodgkins, S. B., Wehr, R. A., Kim, E.-H., Mondav, R., Crill, P. M.,
953 Chanton, J. P., Rich, V. I., Tyson, G. W., and Saleska, S. R.: Methane dynamics regulated by
954 microbial community response to permafrost thaw, Nature, 514, 478–481,
955 https://doi.org/10.1038/nature13798, 2014.

956 McGuire, A. D., Christensen, T. R., Hayes, D., Heroult, A., Euskirchen, E., Kimball, J. S., Koven, C.,
957 Lafleur, P., Miller, P. A., Oechel, W., Peylin, P., Williams, M., and Yi, Y.: An assessment of the
958 carbon balance of Arctic tundra: comparisons among observations, process models, and
959 atmospheric inversions, 9, 3185–3204, https://doi.org/10.5194/bg-9-3185-2012, 2012.

960 Melloh, R. A. and Crill, P. M.: Winter methane dynamics in a temperate peatland, Global
961 Biogeochem. Cycles, 10, 247–254, https://doi.org/doi:10.1029/96GB00365, 1996.

962 Mikhaylov, O. A., Miglovets, M. N., and Zagirova, S. V: Vertical methane fluxes in
963 mesooligotrophic boreal peatland in European Northeast Russia, Contemp. Probl. Ecol., 8, 368–
964 375, https://doi.org/10.1134/S1995425515030099, 2015.

965 Moorcroft, P., Wofsy, S., Dunn, A., and Ise, T.: High sensitiviy of peat decomposition to climate
966 change through water-table feedback, Nat. Geosci., 1, https://doi.org/10.1038/ngeo331, 2008.

967 Natali, S. M., Watts, J. D., Rogers, B. M., Potter, S., Ludwig, S. M., Selbmann, A.-K., Sullivan, P. F.,
968 Abbott, B. W., Arndt, K. A., Birch, L., Björkman, M. P., Bloom, A. A., Celis, G., Christensen, T. R.,
969 Christiansen, C. T., Commane, R., Cooper, E. J., Crill, P., Czimczik, C., Davydov, S., Du, J., Egan, J.

970 E., Elberling, B., Euskirchen, E. S., Friborg, T., Genet, H., Göckede, M., Goodrich, J. P., Grogan, P.,
971 Helbig, M., Jafarov, E. E., Jastrow, J. D., Kalhori, A. A. M., Kim, Y., Kimball, J. S., Kutzbach, L.,
972 Lara, M. J., Larsen, K. S., Lee, B.-Y., Liu, Z., Loranty, M. M., Lund, M., Lupascu, M., Madani, N.,
973 Malhotra, A., Matamala, R., McFarland, J., McGuire, A. D., Michelsen, A., Minions, C., Oechel,
974 W. C., Olefeldt, D., Parmentier, F.-J. W., Pirk, N., Poulter, B., Quinton, W., Rezanezhad, F., Risk,
975 D., Sachs, T., Schaefer, K., Schmidt, N. M., Schuur, E. A. G., Semenchuk, P. R., Shaver, G.,
976 Sonnentag, O., Starr, G., Treat, C. C., Waldrop, M. P., Wang, Y., Welker, J., Wille, C., Xu, X.,
977 Zhang, Z., Zhuang, Q., and Zona, D.: Large loss of CO2 in winter observed across the northern
978 permafrost region, Nat. Clim. Chang., 9, 852–857, https://doi.org/10.1038/s41558-019-0592-8,
979 2019.

980 Nemitz, E., Mammarella, I., Ibrom, A., Aurela, M., Burba, G., Dengel, S., Gielen, B., Grelle, A.,
981 Heinesch, B., Herbst, M., Hörtnagl, L., Klemedtsson, L., Lindroth, A., Lohila, A., Mcdermitt, D.,
982 Meier, P., Merbold, L., Nelson, D., Nicolini, G., and Zahniser, M.: Standardisation of eddy-
983 covariance flux measurements of methane and nitrous oxide, Int. Agrophysics, 32, 517–549,
984 https://doi.org/10.1515/intag-2017-0042, 2018.

985 NILSSON, M., SAGERFORS, J., BUFFAM, I., LAUDON, H., ERIKSSON, T., GRELLE, A.,
986 KLEMEDTSSON, L., WESLIEN, P. E. R., and LINDROTH, A.: Contemporary carbon accumulation in
987 a boreal oligotrophic minerogenic mire – a significant sink after accounting for all C-fluxes,
988 Glob. Chang. Biol., 14, 2317–2332, https://doi.org/10.1111/j.1365-2486.2008.01654.x, 2008.

989 Nisbet, E. G., Dlugokencky, E. J., and Bousquet, P.: Methane on the Rise—Again, Science (80-.).,
990 343, 493 LP – 495, https://doi.org/10.1126/science.1247828, 2014.

991 Nisbet, E. G., Dlugokencky, E. J., Manning, M. R., Lowry, D., Fisher, R. E., France, J. L., Michel, S.
992 E., Miller, J. B., White, J. W. C., Vaughn, B., Bousquet, P., Pyle, J. A., Warwick, N. J., Cain, M.,
993 Brownlow, R., Zazzeri, G., Lanoisellé, M., Manning, A. C., Gloor, E., Worthy, D. E. J., Brunke, E.-
994 G., Labuschagne, C., Wolff, E. W., and Ganesan, A. L.: Rising atmospheric methane: 2007–2014
995 growth and isotopic shift, Global Biogeochem. Cycles, 30, 1356–1370,
996 https://doi.org/10.1002/2016GB005406, 2016.

997 of Sciences Engineering and Medicine: Improving Characterization of Anthropogenic Methane
998 Emissions in the United States, The National Academies Press, Washington, DC,
999 https://doi.org/10.17226/24987, 2018.

1000 Olefeldt, D., Roulet, N. T., Bergeron, O., Crill, P., Bäckstrand, K., and Christensen, T. R.: Net
1001 carbon accumulation of a high-latitude permafrost palsa mire similar to permafrost-free
1002 peatlands, Geophys. Res. Lett., 39, https://doi.org/10.1029/2011GL050355, 2012.

1003 Parmentier, F. J. W., van Huissteden, J., van der Molen, M. K., Schaepman-Strub, G., Karsanaev,
1004 S. A., Maximov, T. C., and Dolman, A. J.: Spatial and temporal dynamics in eddy covariance
1005 observations of methane fluxes at a tundra site in northeastern Siberia, J. Geophys. Res.
1006 Biogeosciences, 116, https://doi.org/10.1029/2010JG001637, 2011.

1007 Post, E., Alley, R. B., Christensen, T. R., Macias-Fauria, M., Forbes, B. C., Gooseff, M. N., Iler, A.,
1008 Kerby, J. T., Laidre, K. L., Mann, M. E., Olofsson, J., Stroeve, J. C., Ulmer, F., Virginia, R. A., and

Wang, M.: The polar regions in a 2{\textdegree}C warmer world, Sci. Adv., 5, https://doi.org/10.1126/sciadv.aaw9883, 2019.

Pugh, C. A., Reed, D. E., Desai, A. R., and Sulman, B. N.: Wetland flux controls: how does interacting water table levels and temperature influence carbon dioxide and methane fluxes in northern Wisconsin?, Biogeochemistry, 137, 15–25, https://doi.org/10.1007/s10533-017-0414-x, 2018.

Raz-Yaseef, N., Torn, M. S., Wu, Y., Billesbach, D. P., Liljedahl, A. K., Kneafsey, T. J., Romanovsky, V. E., Cook, D. R., and Wullschleger, S. D.: Large CO2 and CH4 emissions from polygonal tundra during spring thaw in northern Alaska, Geophys. Res. Lett., 44, 504–513, https://doi.org/10.1002/2016GL071220, 2017.

Rebmann, C., Aubinet, M., Schmid, H., Arriga, N., Aurela, M., Burba, G., Clement, R., De Ligne, A., Fratini, G., Gielen, B., Grace, J., Graf, A., Gross, P., Haapanala, S., Herbst, M., Hörtnagl, L., Ibrom, A., Joly, L., Kljun, N., and Franz, D.: ICOS eddy covariance flux-station site setup: A review, Int. Agrophysics, 32, 471–494, https://doi.org/10.1515/intag-2017-0044, 2018.

Rindskopf, D.: Generalized linear models., https://doi.org/10.1037/13621-009, 2012.

Rinne, J., Riutta, T., Pihlatie, M., Aurela, M., Haapanala, S., Tuovinen, J.-P., Tuittila, E.-S., and Vesala, T.: Annual cycle of methane emission from a boreal fen measured by the eddy covariance technique, Tellus B Chem. Phys. Meteorol., 59, 449–457, https://doi.org/10.1111/j.1600-0889.2007.00261.x, 2007.

Rinne, J., Tuittila, E.-S., Peltola, O., Li, X., Raivonen, M., Alekseychik, P., Haapanala, S., Pihlatie, M., Aurela, M., Mammarella, I., and Vesala, T.: Temporal Variation of Ecosystem Scale Methane Emission From a Boreal Fen in Relation to Temperature, Water Table Position, and Carbon Dioxide Fluxes, Global Biogeochem. Cycles, 32, 1087–1106, https://doi.org/10.1029/2017GB005747, 2018.

Rinne, J., Tuovinen, J.-P., Klemedtsson, L., Aurela, M., Holst, J., Lohila, A., Weslien, P., Vestin, P., Łakomiec, P., Peichl, M., Tuittila, E.-S., Heiskanen, L., Laurila, T., Li, X., Alekseychik, P., Mammarella, I., Ström, L., Crill, P., and Nilsson, M. B.: Effect of the 2018 European drought on methane and carbon dioxide exchange of northern mire ecosystems, Philos. Trans. R. Soc. B Biol. Sci., 375, 20190517, https://doi.org/10.1098/rstb.2019.0517, 2020.

Robertson, A. M., Edie, R., Snare, D., Soltis, J., Field, R. A., Burkhart, M. D., Bell, C. S., Zimmerle, D., and Murphy, S. M.: Variation in Methane Emission Rates from Well Pads in Four Oil and Gas Basins with Contrasting Production Volumes and Compositions, Environ. Sci. Technol., 51, 8832–8840, https://doi.org/10.1021/acs.est.7b00571, 2017.

Röckmann, T., Eyer, S., Veen, C., Popa, E., Tuzson, B., Monteil, G., Houweling, S., Harris, E., Brunner, D., Fischer, H., Zazzeri, G., Lowry, D., Nisbet, E., Brand, W., Necki, J., Emmenegger, L., and Mohn, J.: In situ observations of the isotopic composition of methane at the Cabauw tall tower site, Atmos. Chem. Phys., 16, 10469–10487, https://doi.org/10.5194/acp-16-10469-2016, 2016.

1047 Rößger, N., Wille, C., Holl, D., Göckede, M., and Kutzbach, L.: Scaling and balancing carbon
1048 dioxide fluxes in a heterogeneous tundra ecosystem of the Lena River Delta, 16, 2591–2615,
1049 https://doi.org/10.5194/bg-16-2591-2019, 2019.

1050 Saunois, M., Bousquet, P., Poulter, B., Peregon, A., Ciais, P., Canadell, J. G., Dlugokencky, E. J.,
1051 Etiope, G., Bastviken, D., Houweling, S., Janssens-Maenhout, G., Tubiello, F. N., Castaldi, S.,
1052 Jackson, R. B., Alexe, M., Arora, V. K., Beerling, D. J., Bergamaschi, P., Blake, D. R., Brailsford, G.,
1053 Brovkin, V., Bruhwiler, L., Crevoisier, C., Crill, P., Covey, K., Curry, C., Frankenberg, C., Gedney,
1054 N., Höglund-Isaksson, L., Ishizawa, M., Ito, A., Joos, F., Kim, H.-S., Kleinen, T., Krummel, P.,
1055 Lamarque, J.-F., Langenfelds, R., Locatelli, R., Machida, T., Maksyutov, S., McDonald, K. C.,
1056 Marshall, J., Melton, J. R., Morino, I., Naik, V., O'Doherty, S., Parmentier, F.-J. W., Patra, P. K.,
1057 Peng, C., Peng, S., Peters, G. P., Pison, I., Prigent, C., Prinn, R., Ramonet, M., Riley, W. J., Saito,
1058 M., Santini, M., Schroeder, R., Simpson, I. J., Spahni, R., Steele, P., Takizawa, A., Thornton, B. F.,
1059 Tian, H., Tohjima, Y., Viovy, N., Voulgarakis, A., van Weele, M., van der Werf, G. R., Weiss, R.,
1060 Wiedinmyer, C., Wilton, D. J., Wiltshire, A., Worthy, D., Wunch, D., Xu, X., Yoshida, Y., Zhang, B.,
1061 Zhang, Z., and Zhu, Q.: The global methane budget 2000–2012, Earth Syst. Sci. Data, 8, 697–
1062 751, https://doi.org/10.5194/essd-8-697-2016, 2016.

1063 Saunois, M., Stavert, A. R., Poulter, B., Bousquet, P., Canadell, J. G., Jackson, R. B., Raymond, P.
1064 A., Dlugokencky, E. J., Houweling, S., Patra, P. K., Ciais, P., Arora, V. K., Bastviken, D.,
1065 Bergamaschi, P., Blake, D. R., Brailsford, G., Bruhwiler, L., Carlson, K. M., Carrol, M., Castaldi, S.,
1066 Chandra, N., Crevoisier, C., Crill, P. M., Covey, K., Curry, C. L., Etiope, G., Frankenberg, C.,
1067 Gedney, N., Hegglin, M. I., Höglund-Isaksson, L., Hugelius, G., Ishizawa, M., Ito, A., Janssens-
1068 Maenhout, G., Jensen, K. M., Joos, F., Kleinen, T., Krummel, P. B., Langenfelds, R. L., Laruelle, G.
1069 G., Liu, L., Machida, T., Maksyutov, S., McDonald, K. C., McNorton, J., Miller, P. A., Melton, J. R.,
1070 Morino, I., Müller, J., Murguia-Flores, F., Naik, V., Niwa, Y., Noce, S., O'Doherty, S., Parker, R. J.,
1071 Peng, C., Peng, S., Peters, G. P., Prigent, C., Prinn, R., Ramonet, M., Regnier, P., Riley, W. J.,
1072 Rosentreter, J. A., Segers, A., Simpson, I. J., Shi, H., Smith, S. J., Steele, L. P., Thornton, B. F.,
1073 Tian, H., Tohjima, Y., Tubiello, F. N., Tsuruta, A., Viovy, N., Voulgarakis, A., Weber, T. S., van
1074 Weele, M., van der Werf, G. R., Weiss, R. F., Worthy, D., Wunch, D., Yin, Y., Yoshida, Y., Zhang,
1075 W., Zhang, Z., Zhao, Y., Zheng, B., Zhu, Q., Zhu, Q., and Zhuang, Q.: The Global Methane Budget
1076 2000--2017, Earth Syst. Sci. Data, 12, 1561–1623, https://doi.org/10.5194/essd-12-1561-2020,
1077 2020.

1078 Song, C., Xu, X., Sun, X., Tian, H., Sun, L., Miao, Y., Wang, X., and Guo, Y.: Large methane
1079 emission upon spring thaw from natural wetlands in the northern permafrost region, Environ.
1080 Res. Lett., 7, 034009, https://doi.org/10.1088/1748-9326/7/3/034009, 2012.

1081 Sturtevant, C. S., Oechel, W. C., Zona, D., Kim, Y., and Emerson, C. E.: Soil moisture control over
1082 autumn season methane flux, Arctic Coastal Plain of Alaska, 9, 1423–1440,
1083 https://doi.org/10.5194/bg-9-1423-2012, 2012.

1084 T, V., Eugster, W., and Ojala, A.: Eddy Covariance: A Practical Guide to Measurement and Data
1085 Analysis, in: Springer Atmospheric Sciences Series, vol. 12, 365–376,
1086 https://doi.org/10.1007/978-94-007-2351-1, 2012.

Taylor, M. A., Celis, G., Ledman, J. D., Bracho, R., and Schuur, E. A. G.: Methane Efflux Measured by Eddy Covariance in Alaskan Upland Tundra Undergoing Permafrost Degradation, J. Geophys. Res. Biogeosciences, 123, 2695–2710, https://doi.org/10.1029/2018JG004444, 2018.

Turetsky, M. R., Kotowska, A., Bubier, J., Dise, N. B., Crill, P., Hornibrook, E. R. C., Minkkinen, K., Moore, T. R., Myers-Smith, I. H., Nykänen, H., Olefeldt, D., Rinne, J., Saarnio, S., Shurpali, N., Tuittila, E.-S., Waddington, J. M., White, J. R., Wickland, K. P., and Wilmking, M.: A synthesis of methane emissions from 71 northern, temperate, and subtropical wetlands, Glob. Chang. Biol., 20, 2183–2197, https://doi.org/10.1111/gcb.12580, 2014.

Vellinga, O. S., Dobosy, R. J., Dumas, E. J., Gioli, B., Elbers, J. A., and Hutjes, R. W. A.: Calibration and Quality Assurance of Flux Observations from a Small Research Aircraft*, J. Atmos. Ocean. Technol., 30, 161–181, https://doi.org/10.1175/JTECH-D-11-00138.1, 2013.

Verma, S. B., Baldocchi, D. D., Anderson, D. E., Matt, D. R., and Clement, R. J.: Eddy fluxes of CO2, water vapor, and sensible heat over a deciduous forest, Boundary-Layer Meteorol., 36, 71–91, https://doi.org/10.1007/BF00117459, 1986.

Woodcroft, B. J., Singleton, C. M., Boyd, J. A., Evans, P. N., Emerson, J. B., Zayed, A. A. F., Hoelzle, R. D., Lamberton, T. O., McCalley, C. K., Hodgkins, S. B., Wilson, R. M., Purvine, S. O., Nicora, C. D., Li, C., Frolking, S., Chanton, J. P., Crill, P. M., Saleska, S. R., Rich, V. I., and Tyson, G. W.: Genome-centric view of carbon processing in thawing permafrost, Nature, 560, 49–54, https://doi.org/10.1038/s41586-018-0338-1, 2018.

Wutzler, T., Lucas-Moffat, A., Migliavacca, M., Knauer, J., Sickel, K., Šigut, L., Menzer, O., and Reichstein, M.: Basic and extensible post-processing of eddy covariance flux data with REddyProc, 15, 5015–5030, https://doi.org/10.5194/bg-15-5015-2018, 2018.

Yamulki, S., Anderson, R., Peace, A., and Morison, J. I. L.: Soil CO$_{2}$ CH$_{4}$ and N$_{2}$O fluxes from an afforested lowland raised peatbog in Scotland: implications for drainage and restoration, 10, 1051–1065, https://doi.org/10.5194/bg-10-1051-2013, 2013.

Zhang, Z., Zimmermann, N. E., Stenke, A., Li, X., Hodson, E. L., Zhu, G., Huang, C., and Poulter, B.: Emerging role of wetland methane emissions in driving 21st century climate change, Proc. Natl. Acad. Sci., 114, 9647–9652, https://doi.org/10.1073/pnas.1618765114, 2017.